Intense relativistic electron beam interaction with a cool theta pinch plasma

D. A. Hammer,[a] K. A. Gerber, W. F. Dove,[b] G. C. Goldenbaum,[c] B. G. Logan,[d] K. Papadopoulos, and A. W. Ali

Plasma Physics Division, Naval Research Laboratory, Washington, D. C. 20375
(Received 20 December 1976; final manuscript received 1 November 1977)

Experimental results are presented for the heating of a 4 m long plasma confined by a uniform magnetic field of 4–5 kG by an intense relativistic electron beam. Beam parameters were 0.5–1 MeV, 25–80 kA, 60–70 nsec pulse duration, and electron density of $2\text{–}5\times10^{11}/\text{cm}^3$. The initial plasma density ranged from $5\times10^{13}/\text{cm}^3$ to $4\times10^{15}/\text{cm}^3$ and the electron temperature was 1–3 eV. The lower density cases were partially ionized with $T_e \gg T_i$, and the higher density cases were highly ionized with $T_e \approx T_i$. In all cases, the energy coupled from the beam to the plasma was greater than can be explained by binary collisions between beam electrons and the plasma particles. Beam energy transferred to the plasma ranged from 2–7%/m, and was uniform over the 4 m length of the plasma. Over most of the density range tested, $5\times10^{13}/\text{cm}^3$ to $1.5\times10^{15}/\text{cm}^3$, the plasma heating cannot be explained by classical processes. These results are found to be explained quantitatively by the use of a full nonlinear treatment of the electron-electron two-stream instability in the kinetic regime.

I. INTRODUCTION

The recent availability of electron beam generators[1–5] capable of producing in excess of 1 MJ of relativistic electrons in times of approximately 100 nsec has stimulated a great deal of interest in their application to controlled thermonuclear fusion research. The beam-plasma systems under investigation can be divided into inertially confined and magnetically confined configurations. In the inertial confinement case, present efforts are directed toward the development of beam generators capable of producing the required high power ($\sim 10^{14}$ W), short pulse ($\sim 10^{-8}$ sec) electron beams, and the focusing of such beams onto small targets.[6,7] On the other hand, in magnetically confined systems, it is total energy, rather than power, that matters, so long as the beam pulse duration is less than the energy loss time of the confinement system. Therefore, the 10^{-6} sec pulsed intense relativistic electron beams presently under development[8] are appropriate. The main problems here are the areas of injection, in the case of toroidal systems, and efficient energy deposition in open systems. In the latter case, such as in a high magnetic field, long solenoid,[9] the energy deposition length must be the system length. By contrast, if a beam can be injected into a toroidal system[10] without seriously affecting the energy confinement, the deposition length can be much longer so long as the beam energy is deposited before it is lost by such processes as synchrotron radiation.[11] Therefore, the strength, as measured by the energy deposition length (or time), and the characteristics of the interaction between an intense beam and a plasma will determine the potential applicability of intense electron beams to heating magnetically confined plasmas. In particular, since the classical Maxwellian plasma interaction lengths are too long for efficient deposition in plasmas even in the 10^{17} cm^{-3} density range, collective energy coupling processes are required.

Beam-plasma interaction experiments previously reported[12–26] have shown interaction strengths which imply that a collective interaction must be taking place. The present work investigates the beam-plasma interaction under conditions in which the strength and the characteristics of the physical processes involved could be studied in detail. It was designed so that several of the difficulties in interpreting the results of previous experiments were eliminated. Thus, a 4 m long uniform plasma was used to avoid magnetic field and plasma inhomogeneities. Secondly, the plasma density was high enough so that Thomson scattering could be used to determine plasma electron density and temperature. Finally, the beam current density was kept low enough ($\lesssim 2$ kA/cm^2) so that detailed local magnetic field measurements could be made within the beam channel without probe destruction.

Summarizing the experiment, a 0.5–1 MeV, 25–80 kA, 60–70 nsec electron beam was injected into pre-ionized plasma confined in a 4 m long theta pinch by a 4–5 kG magnetic field. In addition to Thomson scattering and magnetic probes, diagnostics used to study the beam plasma interaction included (1) diamagnetic loops surrounding the plasma, principally to compare with the other diagnostics, (2) visible light, to diagnose the characteristics of the plasma discharge, (3) X-band microwave apparatus, to monitor radiation near the electron cyclotron frequency, and (4) hard x rays, to study the angular spread of the beam. Two different plasma conditions were investigated. In the first one, 100 mTorr of helium was partially ionized to produce a $(0.5\text{–}4)\times10^{14}/\text{cm}^3$, 1–2 eV plasma at the time of beam injection

[a] Present address: Electrical Sciences and Engineering Department, University of California, Los Angeles, Calif. 90024.
[b] Present address: Energy Research and Development Administration, Washington, D. C. 20545.
[c] Present address: Department of Physics and Astronomy, University of Maryland, College Park, Md. 20742.
[d] Present address: Lawrence Livermore Laboratory, University of California, Livermore, Calif. 94550.

 0031-9171/78/2103-0483$00.90

For these experiments, the beam-to-plasma density ratio was 10^{-2}–10^{-3} and the fraction of beam energy coupled to the plasma was 5–7%/m. However, a large fraction of this energy was lost to atomic processes (ionization and line radiation). Preliminary results for these plasma conditions were presented by Goldenbaum *et al.*[24] The second plasma condition was highly ionized hydrogen at a density of $(0.5–4)\times10^{15}/\text{cm}^3$ and temperature of 2–3 eV (electrons and ions). In this case the beam to plasma density ratio was 10^{-3}–10^{-4} and the energy coupling efficiency was 1–2%/m. Since electron and ion temperatures were equal at the time of beam injection, the ion acoustic instability was probably not present. The high plasma density and small neutral fraction made it possible to obtain the heating rate during the beam pulse by Thomson scattering. For plasma density less than $1.5\times10^{15}/\text{cm}^3$, evidence for nonclassical heating was obtained. Furthermore, detailed magnetic probe measurements were made of changes in magnetic field components during the beam-plasma interaction. The axial field showed a rapidly rising (~20 nsec) diamagnetic signal which (on average) continued to rise slowly throughout the beam pulse. The heated cross sectional area after beam passage was more than twice the beam area. The azimuthal magnetic field indicated a net axial current density within the interaction region which was much higher than predicted by return current theory assuming classical dissipation.[27] The anomalously large heating rate and the high net current density can be explained by approximately the same effective collision frequency during the beam plasma interaction. Finally, at the highest densities ($>2\times10^{15}/\text{cm}^3$), classical resistivity return current heating adequately accounts for the observations. Part of the result obtained under the highly ionized plasma conditions were reported in preliminary form by Dove *et al.*[25]

An understanding of these results requires a comparison with expectations based upon the various beam plasma interaction mechanisms which have been discussed.[28] We find that the electron-electron two-stream instability can provide the anomalous resistivities and heating rates observed in the present experiments. If the model used to explain our results applies into the high temperature plasma regime, then it can be expected that longer pulse duration electron beams will have greater overall plasma heating efficiency. This is because, for a given beam-to-plasma density ratio, the instantaneous coupling efficiency increases as the plasma is heated.

The organization of this article is as follows: In order to facilitate comparison with our results, in Sec. II we review intense beam-plasma interaction mechanisms, and previous experimental results. In Sec. III, we describe our experimental apparatus (the plasma source, the electron beam generator, and the diagnostics) as well as the characteristics of the initial plasma and the beam. In Sec. IV, we discuss the experimental results, and in Sec. V they are interpreted in terms of theoretical predictions. Finally in Sec. VI, we discuss the implications of the present work to application of intense relativistic electron beams to controlled fusion in magnetically confined systems.

II. REVIEW OF INTERACTION MECHANISMS AND PREVIOUS EXPERIMENTS

A. Theoretical interaction mechanisms

Coupling of the energy of an intense electron beam into a plasma by collective processes can occur by several mechanisms. Several of these have recently been reviewed by Breizman and Ryutov.[28] We divide the collective mechanisms into two main categories, microscopic and macroscopic. In the first, the beam excites an instability, and the individual electrons interact directly with large amplitude waves which are present at saturation. Thus, the beam transfers its energy to waves, which in turn pass it to the plasma. The instability which has received the most attention in this regard is the electron-electron two-stream instability,[28–35] although other instabilities have also been considered.[28,36] The macroscopic category includes effects which are unique to intense beams, namely, the induced return current,[27,37–40] the presence of large self-fields if the beam is not fully charge neutralized or current neutralized by plasma motion,[28,37,41,42] and the large transverse pressure exerted by the beam against a confining magnetic field, particularly if the beam is rotating across field lines.[23,43,44]

The electron-electron two-stream instability (e-e mode) is driven by the relative drift between beam and plasma electrons. Linear growth rates for unstable waves have been calculated,[29] recalculated,[31] reviewed,[28] and then calculated again[32,36] for ever more "realistic" conditions, meaning conditions which more closely approximate the experiments. For example, the maximum growth rate δ for a "cold" beam satisfying $(n_b/n_p)^{1/3}\gamma \ll 1$ is

$$\delta = \sqrt{1.5}\,\frac{\omega_p}{\gamma}\left(\frac{n_b}{2n_p}\right)^{1/3}(\cos^2\Phi+\gamma_0^2\sin^2\Phi)^{1/3}\ , \tag{1}$$

where n_b and n_p are the beam and plasma densities, respectively, γmc^2 is the beam electron energy, $\omega_p=(n_pe^2/\epsilon_0 m)^{1/2}$ is the plasma frequency, and Φ is the angle of the wave vector $\mathbf{k}$ with respect to the beam propagation direction. The quantities m, $-e$, c, and ϵ_0 are the mass and charge of the electron, the velocity of light and the permittivity of free space, respectively. A beam is "cold" when[34]

$$\Delta v_\parallel/c \cong \bar\theta^2+\Delta E/\gamma^3mc^2 \ll (n_b/\gamma^3n_p)^{1/3}\ , \tag{2}$$

where the parallel velocity spread $\Delta v_\parallel$ is due to either the beam energy spread ΔE or the spread in angle of beam electron velocity vectors relative to the beam propagation direction, represented here by the mean angle $\bar\theta$. If relation (2) is not satisfied, then the growth rate is given by[28]

$$\delta \approx \omega_p\,\frac{n_b}{\gamma n_p}\,\frac{1}{\bar\theta^2}\,\frac{\omega_p^2}{\omega_p^2+k_\perp^2c^2}\ , \tag{3}$$

where $k_\perp = |k|\sin\Phi$, and it is assumed $\bar\theta^2 \gg \Delta E/\gamma^3mc^2$. Similar growth rates can be obtained for strong beams $[(n_b/n_p)^{1/3}\gamma \gg 1]$ in these two limits,[31,32] and for the case when a magnetic field is present, in which case other instabilities are also possible.[36] The linear growth rate tells only a part of the story, however, since it is the

nonlinear limit to which the instability goes which determines the interaction strength and characteristics. Several limiting mechanisms have been discussed, such as quasilinear[28,29,31] and several wave-wave scattering processes,[28,33] and each gives its own interaction length.[12,28,31,33] The energy can be removed from the beam either directly via beam electron-wave interaction, as demonstrated graphically by computer simulations[30,34-36] or by generating anomalous resistivity,[33] or both. Although the predicted interaction lengths vary by many orders of magnitude, they are all short compared with the classical interaction length unless the plasma is too inhomogeneous in the direction of beam propagation.[28] For example, the quasilinear length,[28,31] which is the shortest one, is

$$l \approx 10 \frac{c}{\omega_p} \frac{n_p}{n_b} \frac{T_e}{mc^2} \gamma \bar{\theta}^2 \ , \tag{4}$$

where T_e is the plasma electron temperature. For a $10^{14}/\mathrm{cm}^3$ density, few eV plasma and a $10^{12}/\mathrm{cm}^3$ beam with any mean angle $\bar{\theta}$, l is small compared with c/ω_p, an extremely short length. In fact, it is unreasonably short since the wave energy density used to derive it is sufficiently large so that the weak turbulence approximations used in the derivation are invalid.[28,33] We note that for most of the experiments performed to date, the kinetic growth rate, Eq. (3), should apply, although Thode[34] has obtained reasonably good correlation of theory with experimental results with a modified version of the hydrodynamic formulation.

Turning now to the macroscopic interaction processes, when an intense beam is injected into a plasma, the electric fields induced at the beam front by the rising beam current drive plasma currents back down the beam channel. For a collisionless plasma, when $n_b \ll n_p$ and $\omega_p b/V_b \gg 1$, where V_b is the beam velocity and b is the beam radius, this *current neutralization* is virtually complete throughout the beam cross section.[27,37-40] This result holds with the applied magnetic fields present, as well as without, so long as $\omega_p^2 \gtrsim \omega_c^2$, where $\omega_c = eB_0/m$ is the cyclotron frequency of plasma electrons in the applied field B_0.

Since a plasma is not collisionless, the induced plasma current diffuses out of the beam channel. This has been shown[27] to occur on a time scale $T = [b^2/(c/\omega_p)^2]\tau_c$, where τ_c is the momentum transfer collision frequency of the plasma electrons. $T \gg \tau_c$ in a fully current neutralized beam occurs because energy is delivered inductively from beam electrons to plasma electrons to make up for the energy dissipated (converted to plasma thermal energy) by Ohmic heating.[28,31,45,46] Thode and Sudan[48] have shown that the energy deposited per unit length in the plasma during the beam pulse by the plasma "return" current, Q, is approximately

$$Q = \tfrac{1}{2} LII_b(2 - I/I_b) \ , \tag{5}$$

where I_b is the beam current, I is the *net* current (beam current minus return current) at the end of the beam pulse, and L is the inductance per unit length of the entire beam plasma system. A reasonable limiting value for the net current of a propagating beam is the Alfvén-Lawson critical current, $I_c = 17\,000\ \beta\gamma$, where $\beta = V_b/c$, since a larger current will face severe magnetic self-pinching.[41,47] The time required for the net current to reach $I = I_c$ when $I_b > I_c$ is approximately $T(I_c/I_b)$. This is always a shorter time than for beam energy deposition by binary collisions between beam electrons and plasma particles for beams and plasmas of interest. How much shorter depends upon τ_c, whether it is due to Coulomb collisions or is enhanced by the presence of microturbulence due to instabilities. This microturbulence must be low frequency if it is to affect τ_c, and can occur either parametrically as a result of the e-e mode[28,33] or due to instabilities generated by the relative drift between plasma electrons and ions resulting from the return current flow. In the latter category are such instabilities as electron-ion two-stream and ion acoustic.[28,31,45,46] The interaction length from this process can be estimated as

$$l \sim \frac{(\gamma - 1)mc^2}{eL(dI/dt)} \sim \frac{(\gamma - 1)mc^2\tau_p}{eLI(\tau_p)} \ , \tag{6}$$

where τ_p is the beam pulse duration. It varies directly with the effective collision time τ_c if $\tau_p = T(I_c/I_b)$ is assumed. The energy stored in the magnetic field, $\frac{1}{2} LI^2$ in Eq. (5), also ultimately ends up in the plasma by Ohmic dissipation.[28,48] However, this process can take a much longer time than the dissipation during the beam pulse since instabilities have presumably become much weaker or even stabilized.

The remaining macroscopic collective interaction processes are based upon the large self-fields and transverse pressure of the beam. If the beam is injected into a low pressure neutral gas, then until the gas is turned into a plasma the beam self-electric and magnetic fields can build up, greatly modifying the characteristics of the beam-plasma interaction after gas breakdown.[21,22] For example, magnetic self-pinching[41,47,49] has been observed to heat ions as well as electrons.[21] Similarly, if an intense beam is injected into a plasma or neutral gas with a substantial fraction of its energy in the transverse direction, its transverse pressure can substantially exceed the confining pressure of the applied field. This nonequilibrium situation can result in the generation of large amplitude magnetosonic waves which can also heat both ions and electrons.[43,50] Such expansion waves can also be driven by a rotating beam[23] or by hot plasma if, for example, the plasma electrons are strongly heated by some instability mechanism (e.g., electron-electron two-stream) in a time short compared with the characteristic plasma expansion time.[51] Experiments demonstrating these effects have also been performed.[19,23] Since the experiments to be discussed in this paper did not involve initially neutral gas or a rotating beam, the mechanisms discussed in this paragraph and the experiments designed to test these mechanisms, will not be discussed further.

B. Previous experimental results

The availability of intense electron beams in the mid 1960's soon resulted in experimental studies in which beam propagation characteristics were investigated in plasma and in initially neutral gases.[42,52-56] The first

experiment designed to study the beam-to-plasma energy coupling was that of Altyntsev *et al.*[12] A 2–3 MeV, 10 kA, 50 nsec electron beam ($I_b \ll I_c$) was injected into a 3 m long, magnetic mirror-confined hydrogen or argon afterglow plasma in the density range 10^{11}–10^{14}/cm^3. The beam density was approximately 10^{11}/cm^3 in the interaction volume and the midplane magnetic field was $\lesssim 2.5$ kG. The interaction strength was diagnosed by monitoring the beam propagation efficiency to the end of the interaction region by beam calorimetry, and by using diamagnetic loops to measure the total transverse energy per unit length of the particles (plasma electrons and ions, and beam electrons). The interaction was found to be strongest when the beam and plasma density were comparable, with most of the beam energy failing to reach the end of the system. However, the diamagnetic loops indicated that 10% of the directed beam energy was converted into transverse particle energy, this quantity being optimized at a plasma density of approximately 10^{12} cm^{-3}. Where the rest of the energy went was unknown. Thus, the interaction length for beam loss was $\gtrsim 3$ m for a large enough beam-plasma density ratio. For coupling of beam energy into the plasma, it was perhaps 10 m, much longer than the quasi-linear length given in Eq. (4), but still orders of magnitude shorter than is possible by classical collisional processes. Note that 10% of the beam energy equally distributed among all plasma particles in the system corresponds to tens of keV per electron ion pair. Similar experiments performed by Smith[13] and Okamura *et al.*,[26] also indicated stronger than classical beam-plasma interaction (again using beam calorimetry and diamagnetic loops).

Abrashitov *et al.*,[16] and Arzhannikov *et al.*,[17] followed up the work of Altyntsev *et al.*, with a more completely diagnosed experiment, but still a beam with $I_b \ll I_c$. In particular, at a plasma density of approximately 10^{14}/cm^3, Thomson scattering was used to obtain the plasma transverse electron temperature T_e. The resulting $n_p T_e$ was about six times smaller than the plasma transverse energy inferred from diagmagnetic loops. Other diagnostics in this and other experiments suggest a hot electron component,[15,26] or hot ions,[18] or both, may account for this difference. Since diamagnetic loop measurements were made within 100 nsec of beam injection, other possible explanations for the discrepancy are the residual effects of beam diamagnetism,[57] and magnetosonic waves which have not yet damped.[44,51] The largest signals were observed for $n_b/n_p = 0.05$–0.005. However, at the lower values of $n_p (n_b/n_p > 0.05)$, beam propagation was poor [Fig. 4(b), Ref. 17].

Similar experiments with stronger beams, $I_b/I_c \approx 1$–3 have also been performed. Kapetanakos and Hammer[14] injected a 20–40 kA, 400 keV, 50 nsec beam into a 40 cm long, mirror-confined afterglow hydrogen or helium plasma in the density range 10^{11}–10^{14}/cm^3. Miller and Kuswa[15] used a 50 kA, 350 keV beam of 30 nsec duration and a 30 cm long 10^{12}–10^{14}/cm^3 plasma confined in a uniform magnetic field. Both experiments had beam densities of 10^{12}/cm^3, both used diamagnetic loops as the principal diagnostic for beam energy transferred to the plasma, and both observed maximum values of transfer efficiency of about 5%. However, these maxima were at different density ratios in the two experiments: at $n_b/n_p \approx 1$ for Kapetanakos and Hammer, and at $n_b/n_p \approx 10^{-2}$ for Miller and Kuswa. This difference may have been due to the different beam characteristics or plasma confinement configurations. Kapetanakos and Hammer also found plasma diamagnetism to be independent of magnetic field above 2.5 kG and to scale as B^2 below that field, probably a beam or plasma confinement effect. Miller and Kuswa observed soft x rays at the lower plasma densities confirming the presence of substantially heated plasma electrons. They also made the first mention of magnetosonic oscillations.[44]

In the experiments of Korn *et al.*,[18] and Ekdahl *et al.*,[19] a 10–60 kA, 350 keV, 60 nsec beam ($I_b/I_c \approx \frac{1}{2}$–$3$) was injected into a fully ionized plasma in the density range 10^{12}–5×10^{13}/cm^3. The midplane magnetic field in this 1.6 m long experiment was typically 2.7 kG. The coupling efficiency was highest, up to approximately 20% of the beam energy deposited in the plasma, at the higher beam-to-plasma density ratios, again using diamagnetic loops. However, a neutral particle detector was also used, and it was found that the plasma ions had gained a substantial amount of energy. This was probably due to large amplitude magnetosonic waves since diamagnetic loop oscillations scaled as $B/n^{1/2}$ as predicted by theory.[43,44] In one set of experiments, the energy deposition as a function of current was consistent with return current heating in the presence of ion sound turbulent resistivity.[18] In the other experiments,[19] the heating rate required 10 times that resistivity. The use of a foilless diode[58] in the first set of experiments and an ordinary foil diode[5] in the second may be the explanation for the different interaction characteristics here. As yet unpublished work on the same apparatus by Sethian *et al.*,[59] has shown a very strong dependence of the interaction strength upon beam mean angle as determined by scattering in the anode foil. This result, obtained by both Thomson scattering and diamagnetic loops, at a plasma density of 5×10^{13}/cm^3, points to the presence of the electron-electron two-stream instability,[34] although return current heating may still be present as well.[60]

In an experiment with $I_b/I_c \approx 5$, Miller[20] injected a 600 kA, 100 nsec beam into a 2×10^{13}/cm^3 density plasma ($n_p \approx 20\, n_b$). The most important parameter variation in this experiment was the anode foil thickness, which determines the beam electron mean angle $\bar{\theta}$. This is particularly significant if the two-stream instability is operative.[28,33,34] A decrease by a factor of 10 was observed in diamagnetic loop signals for the thicker foils. The injected beam current density was decreased from a maximum of 6 kA/cm^2 ($n_b \approx 10^{12}$/cm^3) by a factor of $\lesssim 2$ by the thicker foils. Another important result was that beam diamagnetism, certainly substantially increased by the thicker foils, was not dominating the diamagnetic loop signals. The maximum diamagnetic loop signal implied a 1–2% energy deposition efficiency, about 0.25 to 0.5 that expected based upon earlier experiments[12,14–19] at the same value of n_b/n_p.

In summary, all of the beam-plasma interaction ex-

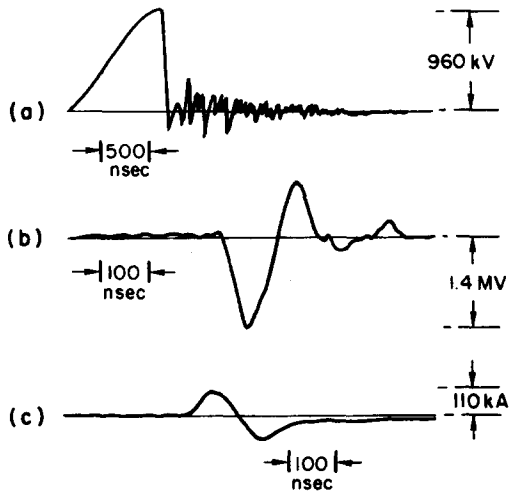

FIG. 1. A sample set of oscillographs of (a) the Marx generator charging the Blumlein pulse forming line, (b) the electron beam diode voltage, and (c) the electron beam current in the diode.

periments reported so far have observed rates of energy deposition in the plasma which imply the presence of one or more collective mechanisms. The results of some of the experiments[12–17,19–21] indicated the presence of the electron-electron two-stream instability, particularly at the lower plasma densities, and others[18,21,22] seemed to imply return current heating. In all of the experiments both mechanisms could have been present. One difficulty in interpreting most of the experimental results is the lack of detailed local measurements of plasma conditions after beam injection. Of the two experiments reported in which Thomson scattering was used to obtain plasma electron density and temperature, one was performed in initially neutral gas,[21] and the other was in a plasma in which conditions would allow both electron-electron two-stream and ion acoustic instabilities to be present.[17] The remaining experiments depended upon nonlocal measurements, mainly diamagnetic loops, to infer beam plasma coupling, and if this is done shortly after beam injection, beam diamagnetism and magnetosonic waves can contribute significantly to the signals. The present experiment has removed some of these difficulties.

III. EXPERIMENTAL APPARATUS AND CHARACTERIZATION OF THE BEAM AND INITIAL PLASMA

The electron beam generator, described in detail elsewhere,[61] utilized a Marx generator[5] charging a Blumlein pulse forming line[5] to produce a 60–70 nsec (FWHM), 500 keV–1 MeV, 25–100 kA electron beam ($I_b/I_c \approx 1$–3). Vacuum field emission diodes, of the type described by Parker *et al.*,[62] were used. Cathodes consisted of flat carbon discs 4–7.5 cm in diameter. The anode was typically a titanium foil 25 μm thick, and was spaced 0.7–1.2 cm from the cathode. Figure 1 shows a sample set of generator oscilloscope traces.

The plasma source in this experiment was a 4 m long, 5 μsec rise time theta pinch, together with a Z discharge preionizer. The theta pinch itself was a 20 cm single turn coil driven by a 60 kJ, 20 kV capacitor bank. The plasma was contained inside a 15 cm glass vacuum vessel which had a base pressure of approximately 10^{-5} Torr. Gas fill pressures ranged from 5 to 200 mTorr of hydrogen, deuterium, or helium depending upon the desired plasma conditions. In order to produce a partially ionized plasma with $n_p \simeq (0.5\text{–}5)\times 10^{14}/\text{cm}^3$, the discharge tube was filled to a gas pressure of 50–200 mTorr, and a Z discharge was fired only a few μsec before the theta pinch. To produce a highly ionized plasma the tube was filled to 5–10 mTorr and the Z discharge was fired about 20 μsec before the theta pinch. Access to the beam generator required a 1 m long drift section between the anode foil and the entrance to the theta pinch coil. A 3 msec risetime magnetic guide field extended over this region. The field amplitude was chosen to match the field at the cathode-anode gap to the theta pinch field at the time of beam injection. To insure that this drift region was highly ionized at the time of beam injection, the primary Z discharge electrodes were the anode foil and electrodes placed just before the theta pinch entrance, as illustrated in Fig. 2. Shortly after breakdown in this drift region, the ionizing discharge within the theta pinch tube was struck from the theta pinch entrance electrodes to the Faraday cup-calorimeter which terminated the beam-plasma interaction region about 0.5 m inside the end of the theta pinch tube. In some of the highly ionized plasma experiments, a 3

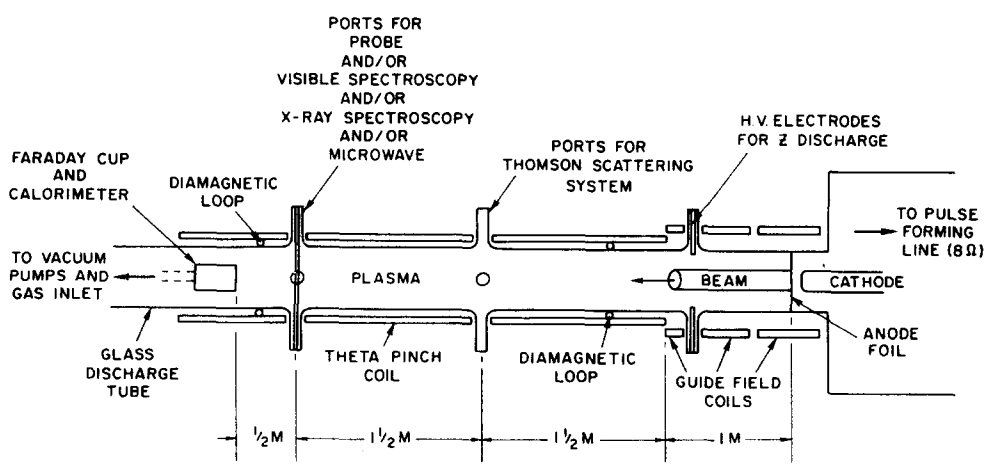

FIG. 2. Schematic of the experiment showing the location of key components and diagnostics.

kJ low inductance capacitor bank was switched into the theta pinch coil, the ringing discharge of which preheated the plasma for subsequent further heating and compression by the theta pinch discharge.

For the bulk of the work to be presented here, a typical electron beam pulse launched from the diode was 2–3 kJ. Of this energy approximately 75% actually entered the theta pinch, the loss occurring mainly at the transition between the slow guide field and the fast theta pinch field regions. Within our shot-to-shot reproducibility, ±15%, all of the beam energy injected into the theta pinch was collected by the Faraday cup-calorimeter 3.5 m downstream. The latter diagnostic, of the type described by Pellinen,[63] allows beam current and total beam energy to be determined. Surveys with witness plates at various axial locations within the discharge tube showed the beam to maintain its initial cross-sectional area (e.g., 40 cm^2 with the 7.5 cm diam cathode). However, at the axial position of the laser diagnostic it was typically distorted into an elliptical form (~3 cm × ~6 cm) with its major axis in a horizontal plane (the plane of the theta pinch slot), and displaced upward and toward the theta pinch slot 1–2 cm. No filamentation instability[64] was observed, apparently stabilized by the 4 kG applied field.

Studies of the beam produced x-ray spectrum and angular dependence from a titanium strip in the guide field region indicated that the beam had an angular spread of about 1 rad.[24] Scattering in the 0.0025 cm titanium anode can account for only a small portion of this (~$\frac{1}{3}$ rad at the 600 keV level used in those studies). Therefore, we postulate that the angular spread was caused by beam interaction with the plasma near the anode foil, or by magnetic field nonuniformities due to, for example, gaps in the guide field coils.

The electron beam was injected into the plasma 1 μsec after peak current was achieved in the theta pinch coil in order to allow the plasma to expand to a reasonably uniform radial profile. This tended to maximize the electron beam energy which could be injected. In the fully ionized plasma case, this also allowed the electrons and ions to equilibrate. At the time of beam injection, electron and ion temperatures were determined to be 2–3 eV, the former by Thomson scattering and the latter by measuring the Doppler broadening of H_α radiation. In the partially ionized case the density was determined by an absolute calibration of the continuum intensity using the model described by Griem,[65] and by Thomson scattering when the density was high enough ($\gtrsim 10^{14}/cm^3$).

The key measurements of plasma electron density and temperature after beam injection into the plasma were made by Thomson scattering[66] of ruby laser light (6943 Å). The laser had a peak power of 400 MW and a pulse width of 30 nsec (FWHM). The scattering volume was a 1.5 cm long by 3 mm diam cylinder of plasma centered on the axis of the theta pinch tube 1.5 m from the entrance. The scattering vector was transverse to the tube axis and the applied magnetic field direction so that $f(v_\perp)$ was measured. The scattered light was analyzed

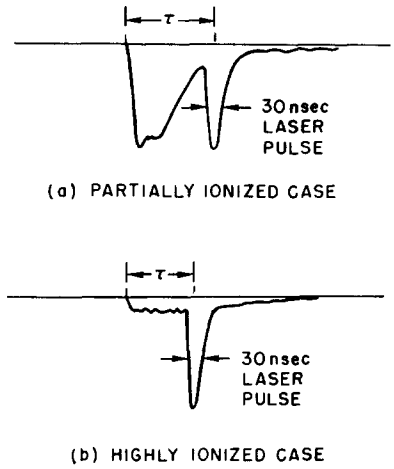

FIG. 3. Sample oscillographs from a typical channel of the Thomson scattering system for the (a) partially ionized and (b) highly ionized cases. The laser timing τ is from the *start* of the beam induced enhanced continuum to the peak of the laser pulse. The large enhanced continuum during the beam pulse in the partially ionized case required $\tau \gtrsim 70$ nsec.

using a five-channel polychromator consisting of a 0.5 m spectrometer, 23 Å spectral width fiber bundles and (RCA 7265) photomultiplier tubes. The entire analyzing system was heavily lead shielded to eliminate signals due to hard x rays from the electron beam. Optical and electrical design parameters and calibration techniques used in the scattering system are available elsewhere.[67,68] Figure 3(a) shows a typical scattered light signal on one of the channels when the plasma was partially ionized helium. The large initial signal occurring during beam injection is optical continuum. This large background signal made density and temperature measurements by laser scattering impossible until about 70 nsec after the start of beam injection. Figure 3(b) shows a typical scattering signal in the highly ionized case. The continuum radiation increased here as well, but only a small amount, serving as a marker for the time of arrival of the beam at the laser scattering port, but not preventing density and temperature measurements during the beam pulse. Figure 4 shows the range of densities and temperatures obtained in one sequence of discharges of the Z discharge-theta pinch systems in which the initial fill was 10 mTorr hydrogen (6.7×10^{14} atoms/cm^3). Although the density varied from about 6×10^{14} cm^{-3} to about 4×10^{15} cm^{-3}, the temperature remained in the narrow range of 2.2–3.2 eV. The large density variation was probably due to nonreproducible desorption of gases from the glass tube walls during the early stages of the theta pinch discharge, and/or nonreproducible compression of the resultant plasma by the theta pinch. The latter could also explain the previously mentioned ±15% variation in beam energy injected into the theta pinch.

Visible light measurements were made on the plasma discharge using 0.25 m and 1 m monochromators together with photomultipliers. For example, in partially ionized helium plasmas, the time history of He-I (4922 Å) and He-II (4686 Å) lines were observed to determine

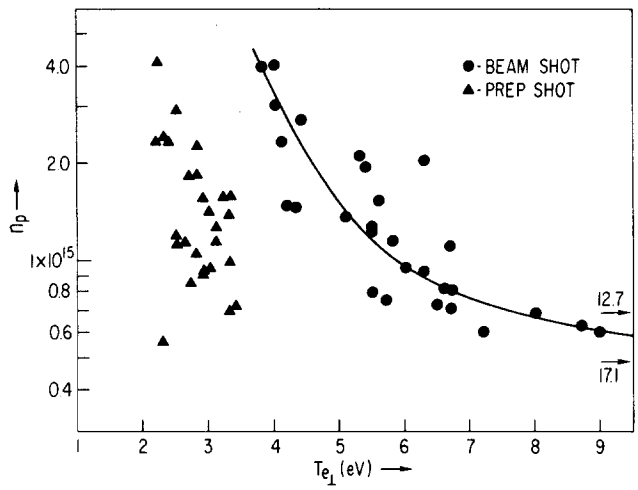

FIG. 4. The range of densities and temperatures (from Thomson scattering) obtained in one sequence of plasma discharges in the highly ionized case with and without beam injection. Arrows indicate two data points with unusually high temperatures. The line is simply to emphasize the trend.

the rate of energy deposition in the plasma during the beam pulse.[24] The 1 m monochromator was used to obtain the Doppler broadened H_α (6561 Å) line width in the highly ionized hydrogen plasma. Stark and Zeeman line broadening were small for our plasma conditions, and resonant charge exchange neutrals emitted easily observable levels of Doppler broadened radiation. The line broadening, assuming Gaussian profiles, indicated an ion temperature of 3 eV at the time of injection of the electron beam. Approximately equal electron and ion temperatures are consistent with collisional relaxation times for our conditions.

Two different types of magnetic diagnostics were used during various phases of this work. Local magnetic field measurements were made in the highly ionized plasma case with a 3 mm diam six turn pickup loop mounted on the end of a 3 mm diam solid copper outer conductor 50 Ω coaxial cable. The loop was moved vertically across the plasma on successive shots inside a 1.25 cm diam 3 mm wall quartz tube which extended all the way across the discharge tube on all shots. In this way the plasma and beam perturbation by the probe housing was the same on all shots. Silicon dielectric fluid within the quartz tube served to suppress electrical discharges within the tube. The presence of the probe housing within the discharge tube (~3 m from the entrance to the theta pinch coil) had a negligible effect on the plasma density and temperature.

The second type of magnetic diagnostic device was a diamagnetic loop, positioned around the glass discharge chamber, which measured the change in total enclosed axial flux. Because of the large voltages induced in the loop by the theta pinch discharge, it was necessary to connect the loop in series with a multiturn, small diameter compensating coil located between the discharge tube and the theta pinch coil. Because of the large inductance of the resulting electrical circuit, the rise time of the loop circuit was approximately 0.5 μsec. Integration time constants of 5 and 10 μsec were used. One such loop was located about 0.5 m inside each end of the theta pinch coil. (See Fig. 2.)

IV. EXPERIMENTAL RESULTS

A. Highly ionized case

Several different experimental runs were taken injecting the electron beam into a highly ionized hydrogen plasma. In the first case to be discussed, a 60–75 kA peak current, 70 nsec (FWHM current pulse), 2 kJ beam reached the Faraday cup-calorimeter. Cathode-anode gap peak voltage was 1.0 MeV, and the beam cross section was approximately 40 cm^2. Figure 4 shows plasma density vs temperature data from Thomson scattering for this run. This figure includes scattering data taken from 40 to 350 nsec after the arrival of the beam front at the scattering port. The data points obtained by firing the full system with the exception of the electron beam which are also shown in Fig. 4 were taken interspersed among the beam shots. Therefore, they are representative of the plasma into which the beam was injected. Note that the density range covered by the prebeam plasma data ("prep shots") and the beam data is virtually the same. It is clear in Fig. 4 that the temperature is strongly density dependent, with the higher density data clearly showing the lowest temperatures, and vice versa, even though the scatter is substantial. (The curve is simply to guide the eye.) Relative errors in these data points are typically ±10% in both density and temperature. In Fig. 5, the temperature as a function of time is plotted. As a result of the functional dependence of temperature on density, the data have been divided into three density ranges based upon the results shown in Fig. 4: $(7\pm3)\times10^{14}/cm^3$, $(1.5\pm0.5)\times10^{15}/cm^3$, and $(3.1\pm1.0)\times10^{15}/cm^3$. The curves drawn for the highest density case will be discussed in the next section. There appears to be no real trend over the time period covered. This is in contrast to our previously published results[25] from a different series of shots, in which rapid post beam cooling seemed to occur. Given the scatter in the present data, the discrepancy is probably due to the small number of shots in the previously published run. The lack of cooling is consistent with the fact that even in the 17 eV shot, electrons moving at the thermal velocity would take 1 μsec to travel half the length of the discharge tube. However, the present data do tend to verify our previous contention that most of the heating occurs in the early part of the beam pulse. The data from the previously published run are included in Fig. 5 in the appropriate density grouping for comparison.

The series of shots just discussed were performed with the five Thomson scattering channels placed symmetrically in wavelength space around the line center at the exit plane of the polychromator. Thus, channels 1 and 2 were located on the red (longer wavelength) side of 6943 Å, 3 was centered on 6943 Å, and channels 4 and 5 were on the blue (shorter wavelength) side. This allowed a slight shift between the line center in prep shots and beam shots to be observed. Such a shift should exist since the beam leaves behind plasma currents in the r, θ plane as well as in the z direction when it exits the

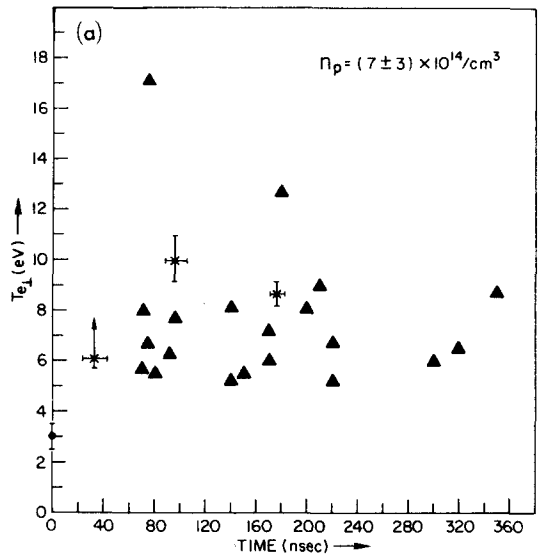

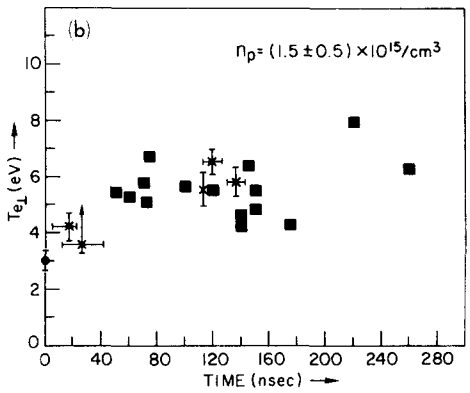

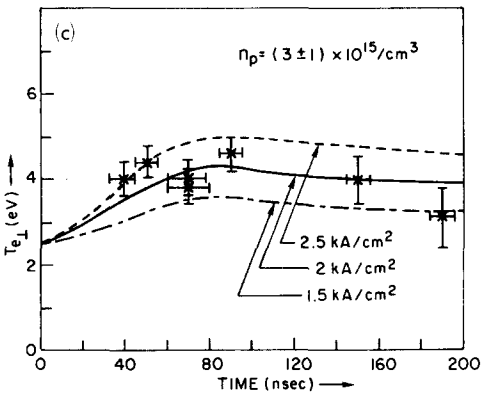

FIG. 5. Plasma temperature as a function of time (from Thomson scattering) for shots having plasma density in the ranges (a) $(7 \pm 3) \times 10^{14}/cm^3$, (b) $(1.5 \pm 0.5) \times 10^{15}/cm^3$, and (c) $(3.1 \pm 1.0) \times 10^{15}/cm^3$. Parts (a) and (b) include data points (shown with error bars) obtained during a previously published run.[25] Arrows on error bars indicate the presence of tails containing an unknown total energy, but estimated to raise the average electron energy to near the top of the arrow. The curves in (c) are obtained assuming classical resistive heating and the plasma current densities shown.

plasma.[25] If the beam plasma system were azimuthally symmetric, the currents in the r, θ plane would be purely azimuthal and the plasma electron distribution would have a drift in the theta direction if the current is due

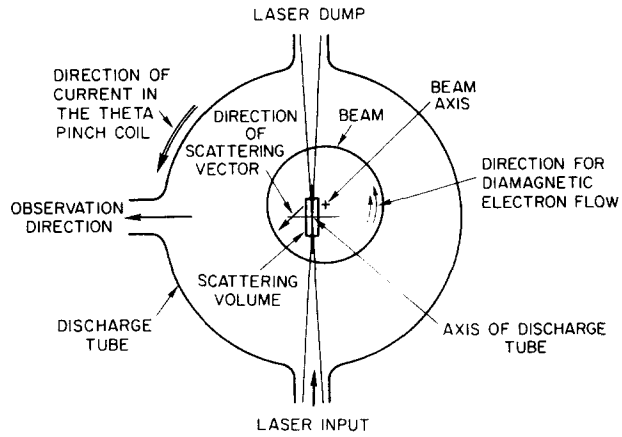

FIG. 6. Simplified interaction geometry at the laser scattering part.

to electrons. Figure 6 is an idealization of the actual unsymmetric geometry showing the scattering volume, the beam position on a typical shot, and the diamagnetic drift direction. Since the beam cross section was not circular, the system was even less symmetric than shown. In the prep shots, the intensities were not symmetric with respect to the laser line center 6943 Å. However, the observed shift to the blue side was a geometric effect determined by the precise placement of the fiber bundles in the focal plane of the polychromator. The average line center obtained from the prep shots was assumed to be at the laser line, 6943 Å. The line center calculation from the data, assuming the line shape is Gaussian, is presented in Appendix A of Ref. 68. During beam shots, the intensity distribution of scattered light changed. The red side intensities were consistently enhanced more than the blue side intensities when compared with the prep shot data. This implies a mean electron velocity vector $\langle \mathbf{v} \rangle$ such that $\mathbf{k} \cdot \langle \mathbf{v} \rangle$ is negative, where $\mathbf{k}$ is the scattering vector, the direction of which is shown in Fig. 6.

Figure 7 shows the observed line center for the beam

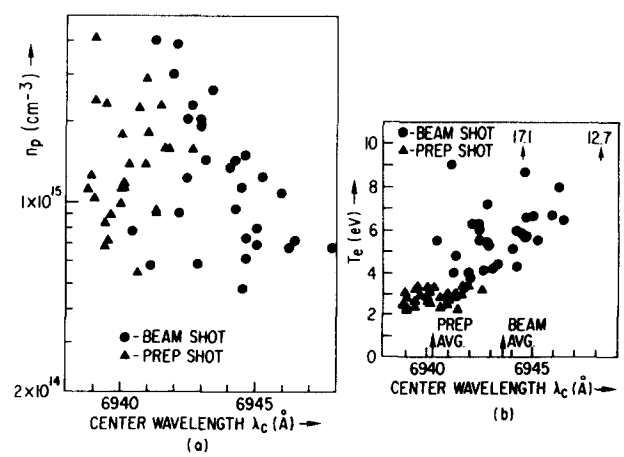

FIG. 7. Calculated scattering line center versus (a) density, and (b) temperature, for beam and plasma shots. Arrows indicate the line center of the 17 eV and 13 eV cases. The tendency for beam shots to have a larger center wavelength is evident in both figures.

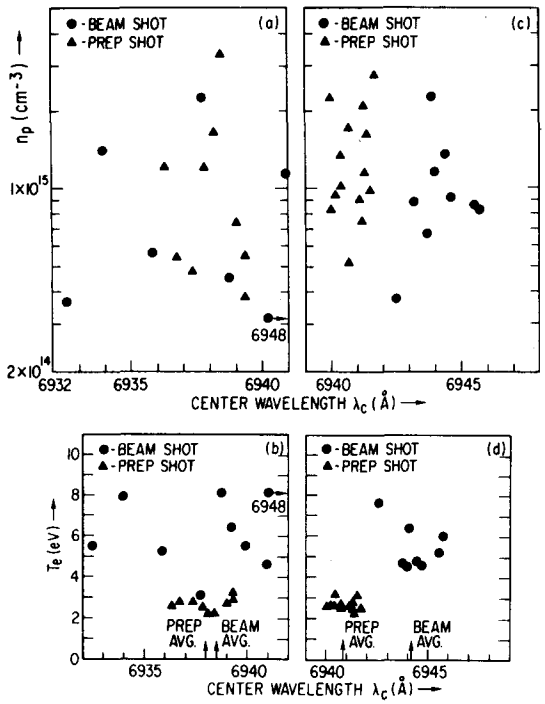

FIG. 8. Scattering line center versus (a) density, and (b) temperature, when only the "upper half" of the scattering volume was viewed. Line center vs density and temperature for the "lower half" of the scattering volume are shown in (c) and (d), respectively.

shots of Fig. 4 as a function of plasma density and temperature, together with the same information for the prep shots of Fig. 4. Errors in the observed intensities produce a typical uncertainity in the deduced line center in each shot of approximately ±1 Å. This is consistent with the calculated standard deviation for the prep shot line centers of 0.93 Å. Figures 7(a) (line center vs density) and 7(b) (line center vs temperature) show no apparent density and temperature dependence for the line center position in the prep shots. On the other hand, for beam shots, Figs. 7(a) and 7(b) show possible trends to greater line center shift for lower density and for higher temperature, respectively.

For the geometric situation shown in Fig. 6, we might expect the drift velocity, if it is a result of plasma electron diamagnetic current flow, to be more evident in the lower part of the scattering volume than the upper assuming symmetric plasma motion *around the beam axis*. This is because the electron drift should be a minimum near the middle of the beam heated plasma, i.e., near the beam axis. Therefore, a series of beam and prep shots were performed looking only at the lower half or only the upper half of the scattering volume. The results for these cases are shown in Fig. 8. The line center as a function of temperature and density for the upper half of the scattering volume, Figs. 8(a) and 8(b), appears completely random relative to the prep shots. This might be expected since the beam axis moved around from shot to shot relative to that volume. However, the beam axis was always above the lower half of the scattering volume, where beam shot line centers were very consistent, as shown in Figs. 8(c) and 8(d). The shift in average line center for prep shots included in Fig. 8 relative to the full scattering volume prep shots in Fig. 7 is believed to be due to differences in the upper and lower halves of the fiber bundles. Thus, it is the relative shift between beam and prep shots which is of interest here.

We note that a 3 Å line center shift implies a drift velocity of 1.3×10^7 cm/sec. At 10^{15} cm^{-3} density, this would imply a plasma electron current of 2–3 kA/cm^2. After beam passage through the plasma, this is an order of magnitude higher than we would expect from plasma diamagnetic currents, or residual net current density.[25] However, any lack of symmetry in the interaction, or residual radial electric fields, might cause gross plasma motion which would not have currents associated with it. Extreme asymmetries of the type suggested by VanDevender *et al.*,[21] as an explanation for apparent drift velocities of approximately 10^8 cm/sec in neutral gas experiments would not be expected in our high density plasma case. However, the magnetic field profiles to be discussed shortly do suggest the presence of asymmetries which may account for our observed drift.

With only two channels on each side of line center in this run, tails in the electron distribution function observed in the previously reported run[25] could not be observed. In that run, one channel was centered at 6943 Å and the remaining four channels were spaced out on the blue side. Recalculation of the density for those experiments gives $(1\pm0.5)\times10^{15}$/cm^3 rather than the previously reported 2×10^{15}/cm^3. That run also included a limited number of shots with deuterium, and evidence for tails on the electron distribution function during the beam pulse, similar to those reported in hydrogen,[25] was observed.

Since data were taken with one or two diamagnetic loops (as described in Sec. III) on most of these shots, it is of interest to compare the Thomson scattering results with the diamagnetic loop signal amplitudes. Since the compensating coil required in our loop circuit made it a few hundred nanosecond rise time diagnostic, a shot by shot comparison with the "early time" Thomson scattering results is not justified. Therefore, we shall consider only the average signal amplitudes for the entire run. In order to obtain a temperature-density product from the diamagnetic loop signal, it is necessary to know the heated cross-sectional area, A_h, since for a simple loop

$$\Delta(n_p \epsilon_\perp) = \frac{B_0 V_{d1} \tau}{\mu_0 A_h (1 - R_L^2/R_w^2)} \text{(mks units)} \ . \tag{7}$$

In this equation $\epsilon_\perp$ is the sum of electron and ion transverse energies per particle, B_0 is the applied magnetic field, V_{d1} is the observed voltage, τ is the diamagnetic loop circuit integration time constant, and R_L and R_w are the loop and conducting wall radii, respectively. The average signal V_{d1} was 9 V (with a 20% standard deviation), with $\tau = 5.6$ μsec $B_0 = 0.4$ W/m^2 and $(1 - R_L^2/R_w^2) = 0.4$. Taking the beam cross sectional area of 40 cm^2 gives $\Delta(n_p \epsilon_\perp) = 6\times10^{16}$ eV/cm^3, or 60 eV per electron ion pair at 10^{15}/cm^3 density. However, we will very shortly see that at least 100 cm^2 is a more reasonable

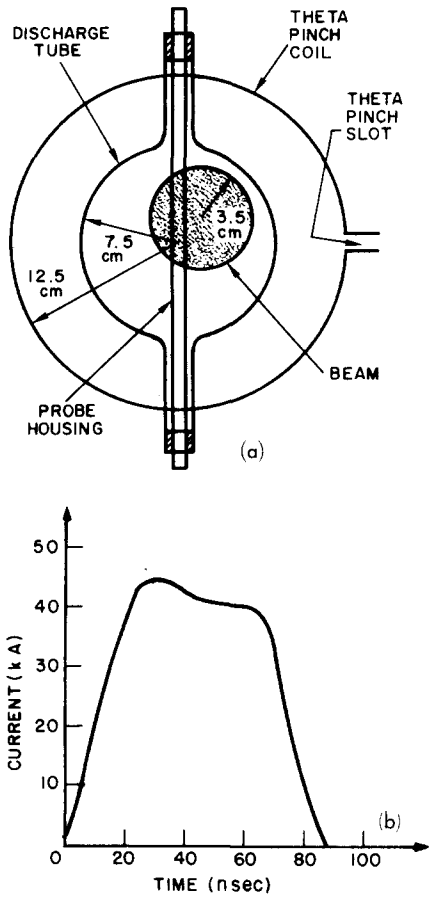

FIG. 9. (a) Simplified interaction geometry at the probe port. (b) Typical Faraday cup oscillogram for the magnetic probe experiment.

estimate of the heated cross-sectional area, giving 24 eV per electron ion pair at $10^{15}/cm^3$. From Figs. 4 and 5 we see that the electron temperature rise according to Thomson scattering is typically only 3 eV at $10^{15}/cm^3$ density. Even assuming equal energies in electrons and ions, the discrepancy here is a factor of 4, remarkably close to the factor of 6 observed by Arzhannikov *et al.*,[17] at about $10^{14}/cm^3$ density. This may be due to energy in rotational drift motion which was noted as a possible explanation for the larger than expected line center shifts. The presence of an energetic tail on the electron distribution function, as predicted by *e-e* instability theory,[30,33] may also explain the discrepancy. Finally, it may be the residual effect of beam diamagnetism.[57] If it is a tail, it must be of order 500 eV or more in order not to collisionally thermalize with the main distribution in the 300–400 nsec covered by the Thomson scattering measurements.

The heated plasma area was obtained from local magnetic field measurements within the interaction region in a separate experimental run. A 40–50 kA peak current, 900 keV peak voltage, 60 nsec beam was injected into the theta pinch. The plasma density was $(1 \pm 0.5) \times 10^{15}/cm^3$ and the temperature approximately 2.5 eV. (The laser scattering system was not in operation during this run. These values for density and temperature were obtained in a series of prep shots taken after the experimental series now under discussion.) Figure 9(a) shows the interaction geometry at the probe port (see Fig. 2) for this run. (The beam position was obtained using solid targets in the beam path at the probe port as well as by x-ray pinhole photography on the probe housing and on a coarse grid of tungsten wires placed at the same axial position.) Figure 9(b) shows a typical Faraday cup waveform for time reference. The results for the change in axial magnetic field (ΔB_z) and the horizontal field (B_x) are shown in Figs. 10(a) and 10(b). Note that in an axisymmetric experiment, B_x would be the azimuthal field component, B_θ. B_x was obtained from the probe signal, dB_x/dt, by the standard technique of a passive RC integrator (having a 2 μsec time constant) at the oscilloscope. However, it was necessary to display dB_z/dt and graphically integrate the oscillograph to obtain ΔB_z because of the voltage induced in the probe by the theta pinch.

At the moment our interest is the diamagnetic area in Fig. 10(a) after the beam has passed. (A diamagnetic ΔB_z signal is negative in the figure.) It is considerably larger than the region in which axial current is flowing, as indicated by the B_x signals in Fig. 10(b). Moreover, since the beam geometry, obtained from targets and x-ray pinhole photography [Fig. 9(a)], and the B_x signals both indicate that the probe is measuring ΔB_z across a chord in the heated plasma rather than a diameter, we infer a disturbed area of 100–125 cm^2 after the beam pulse (see the profiles at 125 or 175 nsec).

The 100 G depth of the diamagnetic well implies a $\Delta(\epsilon_i)$ of about 20 eV per electron-ion pair for $10^{15}/cm^3$ density. Diamagnetic loop amplitudes corresponding to about half this temperature change were observed on these shots (assuming 100 cm^2 heated cross section). We deduce that about 50 J/m of beam energy was deposited in the plasma, assuming isotropy, for a coupling efficiency of 3%/m.

It is interesting to note that the disturbed cross-sectional area indicated in Fig. 10(a) even as early as 50 nsec is considerably larger than the area in which the beam current (and, therefore, the plasma current) is flowing. The speed of cross field energy transport implied by this is $\gtrsim 40$ cm/μsec, a value considerably larger than that obtained in a turbulent heating experiment by Aranchuk *et al.*[69] Thus, not only does beam heating of a plasma avoid skin effect difficulties of ordinary turbulent heating, it also rapidly heats the surrounding volume, possibly by wave energy transport.[69,70]

Turning now to the B_x profiles, there are several characteristics of interest. Firstly, as already noted, the net current implied by this profile during the beam pulse locates the beam in a position consistent with target and x-ray diagnostics (i.e., above the discharge tube axis by about 2 cm). Secondly, the net current position shifts from 2–3 cm off axis to very nearly on axis at the end of the beam pulse. The reason for this is not known, although it may be reflecting a movement of the beam as its current drops from its maximum to zero at the end of the pulse. The magnitude of the net axial current is also of interest. Taking into account the system geometry [Fig. 9(a)], about 500 A of net current is

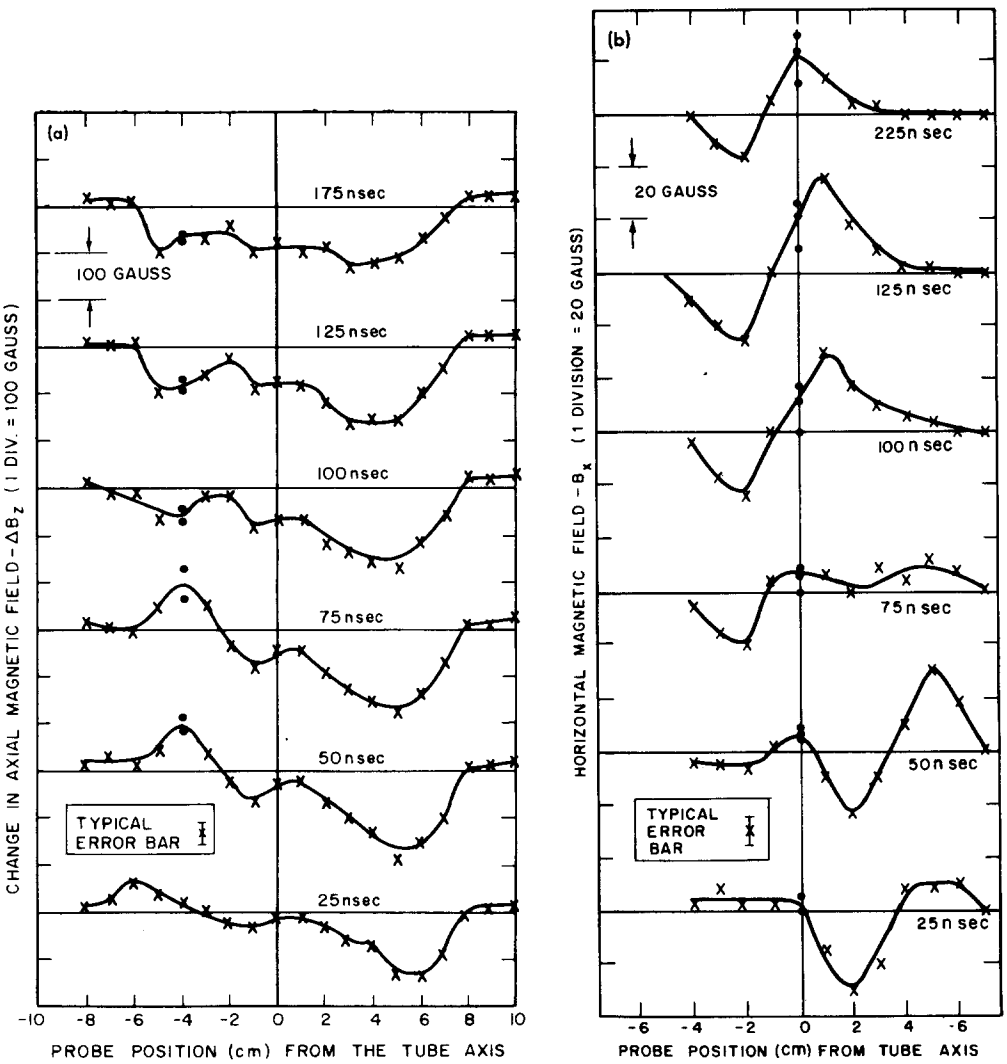

FIG. 10. (a) The change in the axial magnetic field, ΔB_z, and (b) the horizontal magnetic field, B_x, as a function of probe position at various times during the beam-plasma interaction. Shot to shot reproducibility is illustrated by individual data points shown at one radial position in each figure.

implied, i.e., $I_b/100$. This is a factor of 3 greater than would be predicted by sharp beam boundary theory,[27,37] and a factor of 10^3 greater than for the more realistic beam radial density profiles of Kuppers *et al.*,[40] ignoring return current damping.[27] Assuming classical resistivity, the damping time T (see Sec. IIA) for a 3.5 cm radius, 2.5 eV plasma is 7 μsec. Thus, a net current density of 1% might be expected in 70 nsec. The fact that it appears virtually instantaneously (by the end of the beam rise time), and then changes very slowly during the main part of the beam pulse appears to be consistent with a collision frequency greater than 10 times classical at first, and perhaps 2–3 times classical during the next 50 nsec ($T \sim 20$ μsec at 5 eV). These collision frequencies are consistent with values obtained by calculating the heating rates implied by the magnetic profiles.[25]

B. Partially ionized case

The use of a partially ionized plasma adds the possibility of substantial ionization and radiative energy losses to the other processes associated with beam-plasma interaction. If these processes occur fast enough in the target plasma, they must be taken into account in assessing the energy transferred from the beam to the plasma. For example, the ionization energy for hydrogen (H_2) is approximately 15.5 eV and it is approximately 25 eV in helium. In fact, twice these minimum energies are required since line radiation energy losses must be considered. In previously reported results[24] from the present experiment, an approximately 30 kA, 550 keV, 70 nsec beam was injected into a $5\times10^{13}/\text{cm}^3$ density helium plasma with neutral helium density $n_0 \cong 3.5 \times 10^{15}/\text{cm}^3$ (100 mTorr pressure). The applied magnetic field throughout the experimental system was 5 kG in this run, as well as in the partially ionized cases to be discussed later. The plasma density and temperature observed after beam passage were about $7\times10^{14}/\text{cm}^3$ and go to 5 eV. Using these numbers and 40 eV to produce each electron-ion pair to estimate the energy input, we obtain $n_b(3/2\ T_e + 40)/70\ \text{nsec} \approx 5\times10^{23}\ \text{eV/cm}^3 - \text{sec}$ as the average energy deposition rate. This represents a coupling efficiency of 3%/m assuming a heated plasma cross section equal to the beam area (20 cm^2). If the heated area is 2.5 times that area as was the case for the highly ionized experiments discussed in Sec. IIA, the implied coupling efficiency is 7%/m. (The factor of 2.5 is only conjectural in the partially ionized experiments since no magnetic probe scans were taken.)

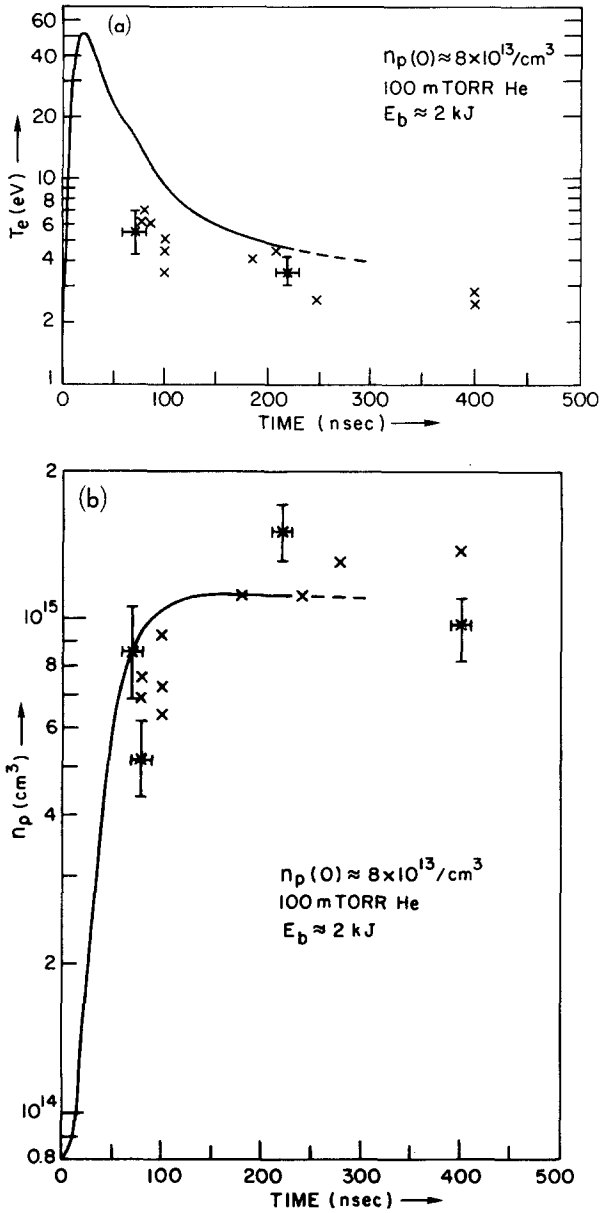

FIG. 11. Results for the 8×10^{13} case showing (a) plasma electron temperature, and (b) density, data as a function of time. Typical error bars are shown. The solid curve is obtained from the numerical model.

Two additional experimental runs were taken in which the beam was injected into partially ionized helium at 100 mTorr pressure. In the first, a 1 MeV, 50 kA peak current, 5 cm diam beam of 70 nsec duration was injected into an $8\times10^{13}/cm^3$ density, 2 eV plasma (the "8×10^{13} case"). In the second run, the beam was 900 keV and 40 kA peak current, and the initial plasma density was $4\times10^{14}/cm^3$, with the remaining parameters being the same (the "4×10^{14} case"). Figures 11 and 12 present the plasma electron temperature and density obtained by Thomson scattering. The time interval covered was 70–450 nsec after beam front arrival at the scattering port, as defined in Fig. 3(a).

The data in Figs. 11 and 12 both show the following characteristics: (1) The plasma density rises from its initial value to about $10^{15}/cm^3$ by the end of the beam pulse, and (2) the temperature is 6–8 eV just after the beam, and falls in about 100 nsec to 3 eV where it stabilizes.

These two runs give average energy deposition rates, $n_p(\frac{3}{2}T_e + 40)/70$ nsec slightly higher than the previously reported case,[24] namely, $(7–12)\times10^{23}$ eV/cm^3 – sec. Because the injected beam energy for these runs was three times that of the previous case, the resulting coupling efficiencies for these higher density cases were lower, namely, 2%/m assuming only the beam area is heated, and 5%/m if 2.5 times that area is heated, as previously discussed.

In order to understand these results a one-dimensional ionization and heating model, similar to that used previously[24] was constructed. It is discussed in detail in the appendix. To summarize, energy is deposited resistively in the plasma at a rate ηj^2, where η is the plasma resistivity and j is the return current density

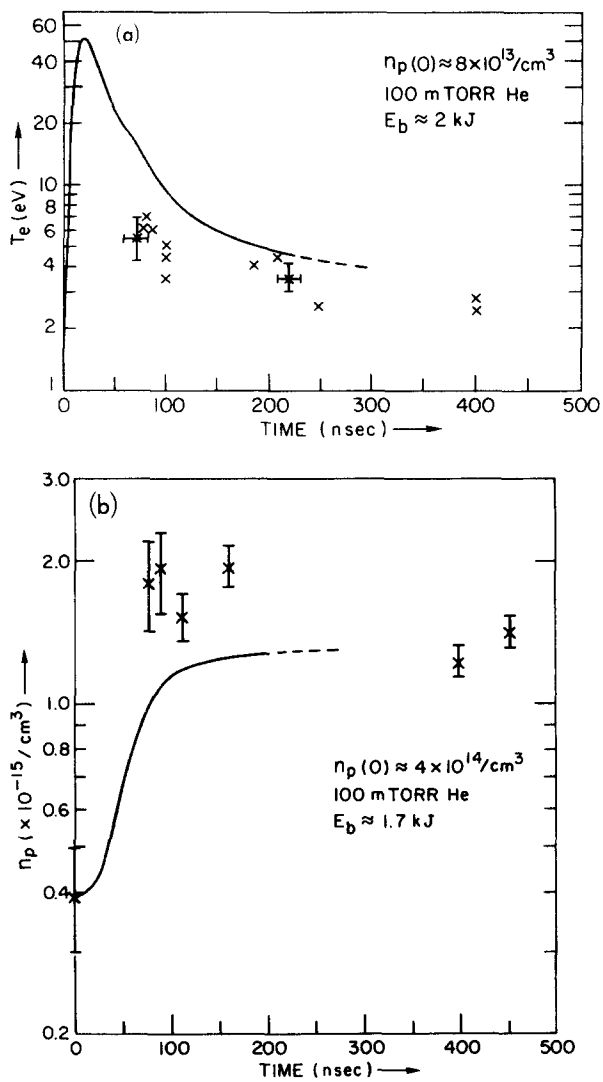

FIG. 12. Results for the 4×10^{14} case showing (a) plasma electron temperature, and (b) density, data as a function of time. Typical error bars are shown. The solid curve is obtained from the numerical model.

in the plasma (assumed equal to the beam current density). The resulting changes in plasma density and temperature are followed in time by solving a coupled set of differential equations [Eqs. (A1)–(A7)] for the densities of neutral, singly, and doubly ionized helium, and for the temperature of these species. The principal energy loss processes included are ionization and line radiation, although Eq. (A5) for the electron energy contains several others. Rate coefficients are temperature dependent as appropriate[71,72] [Eqs. (A11) and (A12)]. The η includes classical [Eq. (A8)], as well as anomalous resistivities due to ion acoustic and e-e mode turbulence [Eqs. (A9) and (A10)], which are discussed in the appendix. The model ignores such plasma dynamic and kinetic effects as expansion and end loss. This is equivalent to assuming the plasma to be spatially uniform. This should be consistent with the low observed temperatures, the short time scale of interest, and classical transport and thermal expansion. The plasma current density is assumed to have a 10 nsec e-fold rise time, a 70 nsec width (FWHM), and a 10 nsec e-fold fall time.

Results obtained from this model are shown together with the experimental data in Figs. 11 and 12. We see that the theoretical plasma temperature shoots up at early times [Figs. 11(a) and 12(a)] while there are relatively few electrons to share the energy input. [This is enhanced by the inverse dependence of the anomalous resistivities on density, Eqs. (A9) and (A10).] The exponential dependence of ionization on temperature, Eq. (A11), means that only when the temperature is above about 10 eV will rapid ionization occur. This occurs in less than 10 nsec in the 8×10^{13} case, and the density rises rapidly, doubling in 25 nsec and redoubling in less than 50 nsec in this case [Fig. 11(a)]. The rate of energy input then decreases (since the anomalous resistivities decrease) and the energy is divided among more electrons, depressing the temperature. By the end of the beam pulse in the 8×10^{13} case, the temperature is only one-third of its maximum value. At this time, the energy input stops (since j decreases to zero), the temperature rapidly decreases to less than 10 eV and further ionization ceases. In the 4×10^{14} case, the temperature peaks at a much lower value. Therefore, the ionization proceeds at a slower rate than in the first case, and the density when the beam (and heating) pulse is over is only three times the initial value. We note that the plasma conditions after the beam pulse are insensitive to small changes in the initial conditions. For example, decreasing the initial electron density to 3×10^{14}/cm^3 changed the density by 2% and decreased the temperature by 1% at $t=100$ nsec.

Comparing the theoretical and experimental results, we see that the theoretical density rises too quickly in the 8×10^{13} case and too slowly in the 4×10^{14} case. Agreement with the final value is quite good in the lower density case, but it is low in the higher density case. In both cases, the experimental temperatures appear to drop to their asymptotic values (~3 eV in both cases) much more quickly than the model predicts. This is probably a result of either nonclassical energy transfer to ions (possibly due to the presence of ion acoustic turbulence), or nonclassical radial energy transport (as by waves). For example, if half the plasma energy at 100 nsec is apportioned to ions (which are $\lesssim 1$ eV from classical heating), temperature agreement would be quite good at that time. Other plasma energy loss processes (such as via impurity radiation, assuming of order 1% nitrogen, carbon and/or oxygen) are too slow to account for the necessary electron cooling rate.

Since we have used only resistive heating in our model, it is reasonable to ask what will happen to these results if nonresistive heating by the electron-electron instability is added. In Sec. V, we shall see that direct heating from this instability can be expected to be greatest near the beginning of the beam-plasma interaction for our experimental conditions. Therefore, in the 4×10^{14} case, we have arbitrarily increased $\dot{Q}$ in Eq. (A5) by 10^{24} eV/cm^3 sec for 10 nsec from $t=6$ to 16 nsec. The resultant density at 100 nsec was 10% higher, and the temperature, although higher at 25 nsec was virtually the same (2% lower) at 100 nsec. We have not carried the numerical calculation beyond 200 nsec since its one-dimensionality and lack of plasma transport mechanisms limit its validity to short times.

A final numerical result to be noted is the deposited energy per electron-ion pair. From Fig. 11 (8×10^{13} case), the plasma energy density, $\frac{3}{2}n_p T_e$, is $\sim 1.5\times10^{16}$ eV/cm^3. An energy of 5.4×10^{16} eV/cm^3 was deposited (*resistively*) in that numerical run. Thus, approximately 4×10^{16} eV/cm^3 remains, implying 40 eV was required to produce each electron-ion pair, as previously assumed. [The approximate equality of the ionization and excitation rate coefficients, Eqs. (A10) and (A12), explains the need for about 1.6 times the 24.6 eV ionization energy for helium.]

In addition to Thomson scattering measurements, we have observed microwave emission in X-band (7–12 GHz) and optical emission of helium I and II lines, and have made diamagnetic loop measurements. The microwave measurements revealed strong emission near the relativistic cyclotron frequency corresponding to the diode voltage and the applied magnetic field (5 kG). This emission occured at the beginning of the beam pulse and had less than 20 nsec full width at half-maximum. The optical line emission, however, could not be accounted for by assuming all the energy deposition occurred during this time. A more uniform deposition rate was required.[24] This leads to the conclusion that the X-band radiation was not associated with the bulk of the energy deposition.

We now take up the diamagnetic loop results, both as independent information and as data to be compared with the results from other diagnostics. This will complete our discussion of the partially ionized case. Figure 13 shows a typical diamagnetic loop signal (after subtracting out the uncompensated portion of the induced voltage from the theta pinch) for the 8×10^{13} case. (It is representative of the other case as well.) Very similar amplitude and shape signals were obtained on the two diamagnetic loops when both were used, indicating the uniformity of the interaction over the 4 m length of the interaction region for this, the partially ionized case, as

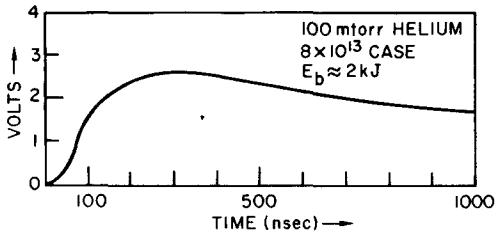

FIG. 13. Typical corrected diamagnetic loop signal for the 8×10^{13} case.

it was in the highly ionized case. (The only difference was that for this case the diamagnetic loop signal at the upstream end of the system sometimes showed oscillations of the type to be discussed later.) Because of the slow response time of the diamagnetic loop circuit, the signal voltage is not simply related to the instantaneous plasma energy density as measured by Thomson scattering. In order to obtain a comparison we assumed the theoretical density and temperature time histories as shown in Fig. 11 to be correct, and approximated the product $n_p T_\perp$ by a triangular-shaped transverse energy pulse of full width 100 nsec and peak of 6×10^{16} eV/cm^3 at $t = 50$ nsec. We then calculated the expected oscilloscope voltage as a function of time taking a 22 μH compensating coil, a 50 Ω cable terminated in 50 Ω, and an $RC = 10$ μsec integrator at the oscilloscope. The resultant wave form was qualitatively similar to the experimental trace in Fig. 13, but was a factor of two too small.

The triangular-shaped (in time) pulse of diamagnetism used in the calculation just described was chosen as an approximation to the plasma diamagnetism implied by Fig. 11. However, it could just as well represent beam diamagnetism since $n_b \approx 4\times10^{11}$/cm^3 (2 kA/cm^2) would require only 150 keV transverse energy per beam electron to produce 6×10^{16} eV/cm^3. In the final series of shots to be discussed in this paper, 12 cm^2 and 40 cm^2 beams at approximately 900 keV were injected into partially ionized hydrogen at less than 5×10^{13}/cm^3 and approximately 1 eV. The beam current density was in the range 1.2 to 3.5 kA/cm^2 for the smaller area beam and was about 1.2 kA/cm^2 for the larger beam. (Density

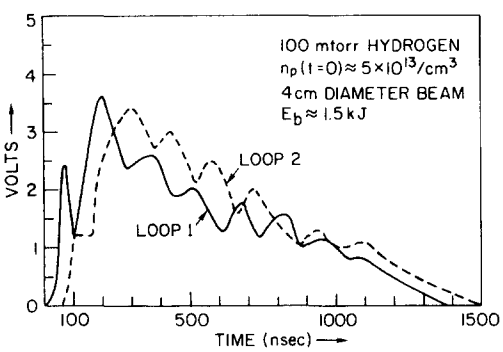

FIG. 14. Diamagnetic loop signals from loops at both ends of the theta pinch in a partially ionized hydrogen experiment. Oscillations were present in most hydrogen cases.

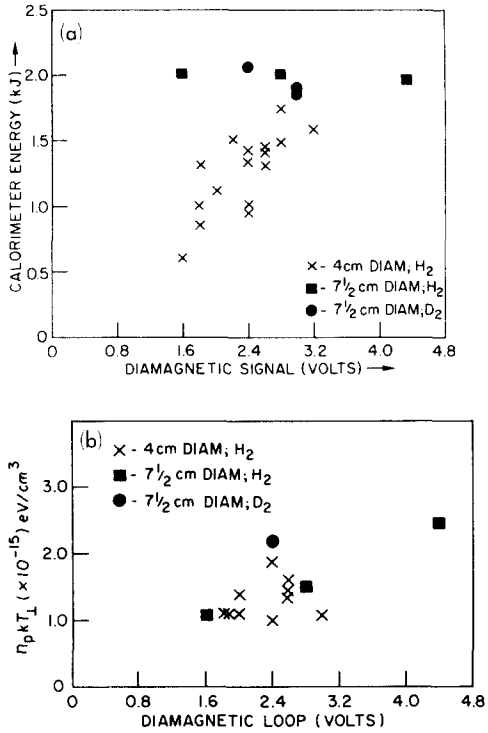

FIG. 15. Comparison of (a) diamagnetic loop amplitude and beam energy on the calorimeter, and (b) diamagnetic loop amplitude and $n_p T_\perp$, obtained from Thomson scattering, for partially ionized hydrogen experiments.

and temperature as a function of time from laser scattering gave results quantitatively similar to the partially ionized helium data shown in Figs. 11 and 12. There were, however, too few shots at any given beam condition to draw a graph similar to those figures for these shots.) Figure 14 shows typical diamagnetic signals for these shots. In Fig. 15(a) we plot the amplitude of the diamagnetic loop near the calorimeter versus the calorimeter energy. The smaller area beam shows a clear trend toward loop signal being proportional to propagated beam energy. (Since the beam voltage pulse duration was virtually the same for all shots plotted, only the current varies to produce the variation in beam energy.) The larger area beam data do not show this trend.

In Fig. 15(b), $n_p T_{e\perp}$ obtained from laser scattering is plotted against diamagnetic loop amplitude for those shots from Fig. 15(a) for which scattering data were taken. There is some indication here that plasma energy after the beam pulse and the diamagnetic loop signal are correlated. As in the helium cases, the diamagnetic loop is indicating more than an order of magnitude more transverse energy than the laser scattering, presumably for the same reasons. The data of Fig. 15 (a) suggest that beam diamagnetism cannot be ruled out as a contributing factor, at least for the smaller area beam. However, an equally allowable explanation is stronger beam-plasma interaction for the higher current density beams.

Returning to Fig. 14, we note that both signals show oscillations with the same period, probably the magnetosonic oscillations previously discussed.[15,19,23,44,51] The

more prominent oscillations on the diamagnetic loop signals here as compared with the helium shots (e.g., Fig. 13) may be a result of the magnetosonic waves being damped by more collisions in the helium case.[44] In addition, we see that the amplitudes of the two signals in Fig. 14 are virtually the same, again indicating the uniformity of the interaction over the entire system length.

V. THEORETICAL CONSIDERATIONS

In this section we address the questions of what beam-to-plasma energy transfer mechanisms are expected under the conditions of our experiments, and how much energy we expect the beam to lose according to the appropriate theory. We first present a qualitative discussion of the most probable loss mechanisms (direct electron-electron two stream and return current heating), including their time dependent characteristics. These are subsequently applied to our experiments.

According to linear theory two types of waves are expected during intense beam-plasma interaction. The first type corresponds to Langmuir waves excited by electron-electron two stream instability (e-e mode) with wave length of the order c/ω_p. We refer to the energy density of these waves as W_1. The second type corresponds to ion acoustic waves, W_a which can be excited when the induced return current drives electron-ion instabilities (e-i modes). An approximate criterion for the excitation of such instabilities is $v_d/c_s \gg T_i/T_e$ ($v_d > c_s$ if $T_i \ll T_e$), where $c_s = [(T_e + T_i)/M]^{1/2}$ and v_d is the plasma electron drift velocity relative to the mass M of the ions. Two energy transfer mechanisms are, therefore possible. One is the direct interaction of the beam electrons in resonance with the waves W_1 [i.e., $\omega_p - c(\mathbf{k}\cdot\mathbf{p}/|\mathbf{p}|) = 0$, where p is the beam electron momentum vector]. The second is scattering of the plasma electrons forming the return current on W_a, which results in anomalously high resistance. In order to compute the energy transfer rates, the wave energy levels W_1 and W_a must be known. The computation of these levels been the most controversial aspect of beam-plasma heating.

An extensive amount of work has focused on the determination of W_1 and the associated energy coupling length (l) on the basis of convective quasilinear theory.[28,29,31] Such considerations produced the length given by Eq. (4). As discussed in Sec. II experiments have shown this to be much too short. This is physically expected since for any parameters of interest, the magnitude of W_1 violates the assumptions of quasilinear theory.[33] An alternative possibility is that the amplitude W_1 is limited by nonlinear wave-wave interactions. The general idea of this concept is that beyond a certain level of W_1, wave energy is transferred into a nonresonant region. A stationary state can then be achieved where the energy transfer from the beam to the (resonant) Langmuir waves is balanced by the transfer of wave energy to the nonresonant region. As a result, W_1 is maintained at a low level while dissipation occurs only in the nonresonant regions. The energy loss rate for the beam electrons is then proportional to $2\delta W_1$, where δ is the instability growth rate given by Eq. (3). Early attempts to apply these concepts to beam-plasma experiments[28,31] were confined within the framework of validity of weak turbulence theory (i.e., the real part of the frequency obeys the linear dispersion relation). These efforts still failed to reconcile the differences between theory and experiment. However, Papadopoulos[33] showed that for any resonable parameters applicable to present day intense beam plasma interaction experiments the weak turbulence theory is not valid and inclusion of nonlinear frequency shifts is important. It was shown that when $W_1/n_p T_e > (T_e/mc^2)^{1/2}$, the wave spectrum becomes unstable to a secondary instability similar to the oscillating two-stream instability.[33,73] (Within this context, the instability is also known as the modulational or modified decay instability.) This process transfers energy to electron plasma waves with lower phase velocities (shorter wavelengths) and associated low frequency ion waves. The lower phase velocity plasma waves can be linearly Landau damped by the tails of the plasma electron distribution function. Note that these wave processes viewed in configuration space correspond to plasma waves trapped in low density regions and have been given the name of plasma solitons, cavitons, and spikons.[74] It has been shown[75] that they are equivalent representations of the oscillating two-stream instability. It should also be noted that among the new concepts introduced by the strong turbulence theory is the possibility of exciting ion waves W_a created directly by the ponderomotive force exerted on the plasma by W_1 even in the absence of return current driven instabilities (e-i modes).

On the basis of this model, the details of which are available elsewhere,[33] the time sequence of events is as follows: Upon injection of the beam into the plasma, the waves W_1 grow rapidly until they reach a level such that their removal from the instability region is faster than the e-e instability growth. This is given by [see Eqs. (25)–(26) of Ref. 33]

$$\frac{W_1^{\max}}{n_p T_e} = \frac{M}{m}\left(\frac{\delta}{\omega_p}\right)^2 \Lambda^2 \ ,$$

$$\Lambda = \ln\left[\frac{\delta}{\omega_p}\left(\frac{M}{m}\right)^{1/2} \frac{n_p T_e}{W_2(t=0)}\left(\frac{W_1^{\max}}{n_p T_e}\right)^{1/2}\right] \ . \tag{8}$$

They subsequently decay to Langmuir waves nonresonant with the beam electrons (W_2) and modified ion plasma wave (W_a). This is illustrated in Fig. 16. A quasi-stationary state can be established on the basis of the following arguments: The presence of finite amplitude ion waves W_a can produce an ac resistivity for waves near the plasma frequency with effective collision rate ν_H^*, as discussed by Dawson and Oberman,[76] and a dc resistivity[33,77] with rate $\nu_0^* = \overline{k\lambda_D}\,\nu_H^*$, where $\overline{k\lambda_D}$ is the characteristic wavenumber Debye length product for the ion waves. When

$$\nu_H^* = 2\delta \ , \tag{9}$$

the e-e instability is nonlinearly stabilized and the energy deposition rate via waves $d\epsilon_1/dt$ will be given by

$$\frac{d\epsilon_1}{dt} = \nu_H^* W_1\left(1 + \frac{\partial \omega D}{\partial \omega}\right) = 4\delta W_1 \ , \tag{10}$$

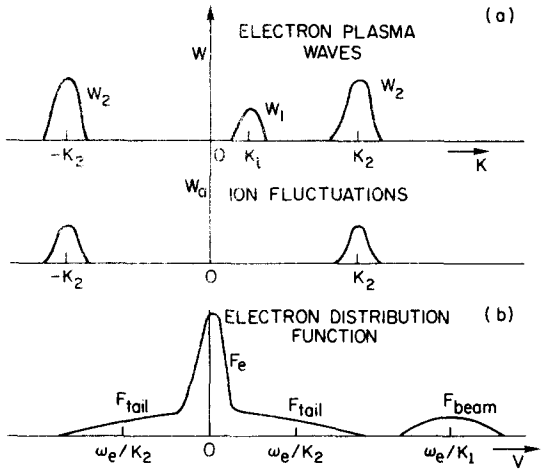

FIG. 16. Nonlinear quasi-stationary state of the beam-plasma system. (a) Spectral distribution of electron plasma (Langmuir) waves (W) and ion waves (W_a). (b) Schematic of the electron distribution function including the slowly drifting plasma component, plasma electron tails, and beam electrons.

where D is the dielectric function of the plasma. In addition to this, the presence of the dc collision frequency ν_0^* will provide an energy deposition mechanism due to the return current $j = n_p e v_d$. This will be given by

$$\frac{d\epsilon_2}{dt} = \eta^* j^2 = \frac{4\pi\nu_0^*}{\omega_p^2} j^2 = \frac{4\pi}{\omega_p} \overline{k\lambda_D} \frac{2\delta}{\omega_p} j^2 \quad . \tag{11}$$

Notice that if the Coulomb collision rate ν_c is greater than ν_H^* or ν_0^*, then it replaces them in these arguments. Furthermore, if an e-i instability is present, W_a, and therefore the effective collision frequencies might have to be determined by other considerations.[28] The energy levels W_1 and W_2 are determined by the condition that the ion waves are marginally stable. This gives [Ref. 33, Eqs. (39)–(44)]

$$\frac{W_1}{n_p T_e} = 4 \frac{\nu_H^*}{\omega_p} = 8 \frac{\delta}{\omega_p} \quad . \tag{12}$$

It should be noted that these relations have been verified by computer simulations using particle and mode coupling codes.[78]

We now proceed to apply these concepts to the present experiment. In order to be more precise quantitatively we first select the case where the beam ($n_b \approx 5\times10^{11}$/cm^3) was injected into a highly ionized plasma with density $(7\pm3)\times10^{14}$/cm^3 and initial temperature $T_e \approx T_i \approx 3$ eV. For these parameters, e-i instabilities are not expected, since $v_d \ll v_e$. We consider a beam current density pulse which rises in 20 nsec to the experimentally observed peak value, is flat for 50 nsec, and then drops instantaneously to 0, and see if Eqs. (8)–(12) predict the energy deposition data and the field diffusion timescale as measured by the laser scattering and magnetic probes. The time $\tau = 0$ is the time the beam front arrives at the particular diagnostic port. We compare the observation first with the approximate analytic results, and then the results of a numerical solution of the nonlinear equations.[78]

For the parameters of this experiment and for the energy deposition during the initial stage we find from Eq. (8) that $W_1^{\max}/n_p T_e = 0.32$. The actual energy loss of the beam is given by $\Delta\epsilon_0 = W_1^{\max}(1 + \partial\omega D(\omega, k)/\partial\omega) \approx 2W_1^{\max} \approx 1.36\times10^{15}$ eV/cm^3. This energy is delivered during a 5 nsec time interval around $\tau = 20$ nsec since the instability does not start ($2\delta < \nu_c$) until $\tau \approx 15$ nsec. At this time both ν_H^* and ν_0^* reach a maximum and then relax towards their quasi-stationary values. For the case under consideration these are given by $W_1/n_p T_e \approx W_2/n_p T_e \approx 8\delta/\omega_p \approx 2\times10^{-2}$, $W_a/n_p T_e \approx 10^{-4}$ and $\overline{k\lambda_D} \approx 0.1$–$0.2$ (for $\gamma = 3$ and $\bar{\theta} \approx 1/3$). With these values we find that for the rest of the beam pulse the energy deposition rate due to wave damping, given by Eq. (10), is

$$\frac{d\epsilon_1}{dt} = 4.6\times10^{23} \frac{\text{eV}}{\text{cm}^3 - \text{sec}} \quad ,$$

while the one due to the return current, Eq. (11), is

$$\frac{d\epsilon_2}{dt} = 2.5\times10^{23} \frac{\text{eV}}{\text{cm}^3 - \text{sec}} \quad .$$

The total energy lost by the beam according to this model is about 3.5×10^{16} eV/cm^3. For a 40 cm^2 beam, this gives 1.4×10^{18} eV/cm during the entire pulse. This is to be compared with 5×10^{17} eV/cm deposited energy measured by laser scattering assuming 100 cm^2 heated plasma cross section, [Fig. 5(a)] and 2×10^{18} eV/cm from the diamagnetic loop average.

We have checked the conclusions of the simplified analytic model by numerically solving[78] the exact mode coupling equations which are derived in Ref. 33, including the effect of finite beam rise time and classical collisional damping. The results for the energy deposition, low frequency resistivity, and wave spectrum as a function of time are shown in Figs. 17–19. The analytic results are included for comparison and are seen to be consistent with the discussion we have presented. Note that the computational results for energy deposition

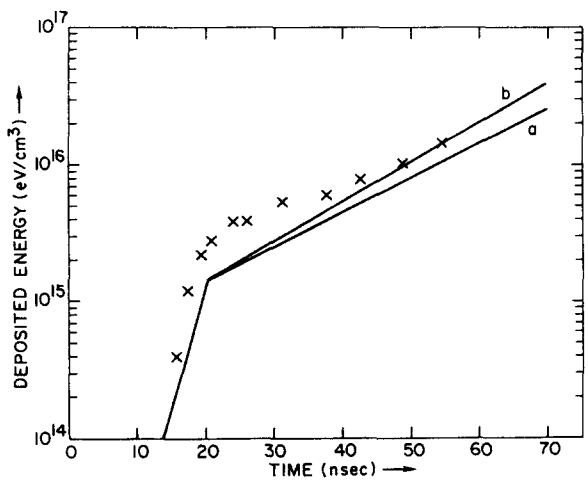

FIG. 17. Beam energy deposition rate as a function of time for the highly ionized case. Continuous lines are averaged results from the approximate analytic theory. Line (a) represents deposition due to wave damping, while (b) is the total including the resistive heating. The points are results from the numerical solution of the exact mode coupling equations including only wave damping.

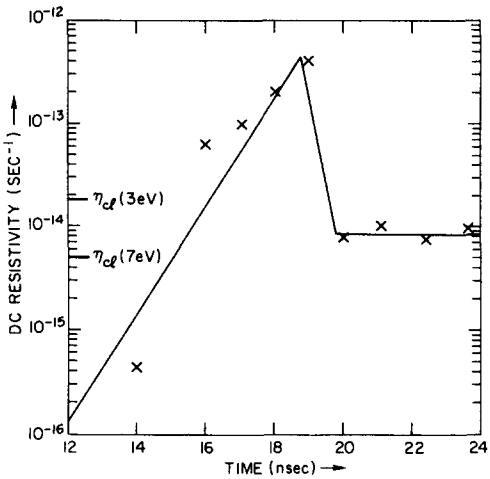

FIG. 18. Time dependence of anomalous resistivity for the case considered in Fig. 17. Again the line is from the analytic model while the points are from the numerical experiments averaged over a ~1 nsec time interval.

(Fig. 17) do not include resistive heating contributions. From Fig. 18 we can see an early time resistivity which is more than an order of magnitude larger than classical, and a later time resistivity of about twice the classical value, as required to explain the magnetic probe results (Fig. 10). The high and low frequency wave spectra during the various stages of the interaction, shown in Fig. 19, demonstrate that modes with phase velocity in resonance with the beam (marked by +) dominate only at early time.

In the higher density highly ionized experiments for which results are shown in Fig. 5 [i.e., $n_p = (1.5 \pm 0.5) \times 10^{15}/\text{cm}^3$ and $n_p = (3.1 \pm 1) \times 10^{15}/\text{cm}^3$], $2\delta < \nu_c$ for all time during the pulse assuming that $T_e = 3$ eV and $\bar{\theta} \approx 1/3$, therefore, we do not expect the e-e instability to be excited. For the case $(3.1 \pm 1) \times 10^{15}/\text{cm}^3$, as shown in Fig. 5(c), classical heating by dissipation of the return current can account for the observed increase in temperature. However, this is not true for the $(1.5 \pm 0.5) \times 10^{15}/\text{cm}^3$ case. At this stage we can only speculate that perhaps some nonuniformity in the beam current density can produce a sufficient local heating at early time, to allow $2\delta > \nu_c$ and the e-e instability to be excited.

We now proceed to examine the partially ionized results. For the $4 \times 10^{14}/\text{cm}^3$ case with a 40 kA, 900 keV beam, we have that the initial growth rate is given by $\delta = 3.8 \times 10^{-3}\, \omega_p$. Therefore, from Eq. (12) we obtain an energy delivered in the initial stages of the instability of $\Delta\epsilon_0 = 5 \times 10^{15}$ eV/cm^3. At this point we must consider the effect of substantial temperature changes due to heating and the increasing plasma density due to ionization of the $3 \times 10^{15}/\text{cm}^3$ neutrals present in the system. If we combine Eqs. (10) and (12), we obtain a wave energy deposition rate appropriate for this case

$$\frac{d\epsilon_1}{dt} = \frac{2 \times 10^{23}\, T_e(t)}{(n_p(t)/4 \times 10^{14}\ \text{cm}^{-3})^{3/2}} \frac{\text{eV}}{\text{cm}^3 - \text{sec}} \ . \tag{13}$$

(In this equation, T_e is an effective temperature, since there may be tails, as shown in Fig. 16.) In Fig. 12 we saw that the time for significant increase in density in this case is comparable to the pulse duration for initial energy deposition rates of order 10^{24} eV/cm^3 – sec. Therefore, it is reasonable to assume small density change and take $n_p(t) \approx 5 \times 10^{14}/\text{cm}^3$. We can also approximate $T_e(t)$ by 10 eV. This gives an "average" value for the wave energy deposition rate of

$$d\epsilon_1/dt \approx 1.5 \times 10^{24}\ \text{eV/cm}^3 - \text{sec} \ ,$$

a result consistent with our use of Fig. 12 for guidance. Thus, the energy deposition via waves during the remaining beam pulse is $\Delta\epsilon_1 \approx 7.5 \times 10^{16}$ eV/cm^3. Using Eq. (11) to obtain a resistive energy deposition rate equivalent to Eq. (13), we obtain

$$\frac{d\epsilon_2}{dt} = \frac{1.6 \times 10^{17} j^2\,(\text{A/cm}^2)}{(n_p/4 \times 10^{14}\ \text{cm}^{-3})^{3/2}} \ , \qquad \approx 5 \times 10^{23} \frac{\text{eV}}{\text{cm}^3 - \text{sec}} \ , \tag{14}$$

the latter number being an average rate during the pulse. The resistively deposited energy, therefore, totals $\Delta\epsilon_2 \approx 2.5 \times 10^{16}$ eV/cm^3. Summing the three components, the energy deposition according to the present model comes to 1.0×10^{17} eV/cm^3. Averaging this over the full beam pulse width (70 nsec), we obtain an average energy deposition rate of 1.5×10^{24} eV/cm^3 – sec, 30% greater than the value estimated for this case from Fig. 12 (including the 40 eV ionization energy and the 2.5 area factor) in Sec. IVB.

Since the plasma conditions in the partially ionized cases allow the possibility of ion acoustic turbulence, we must consider the contribution which this instability may make to the heating. From the work of Zavoisky *et al.*,[79] it is possible to obtain a value of the anomalous resistivity due to ion acoustic turbulence, η_{ia}, for $v_e > v_d > c_s$. This value, in a form appropriate for comparison with the coefficient of j^2 in Eq. (14), is

$$\eta_{ia} = \frac{1.8 \times 10^{17}}{(n_p/4 \times 10^{14}\ \text{cm}^{-3})^{1/2}} \frac{\text{eV}}{\text{cm}^3 - \text{sec} - \text{A}^2} \ . \tag{15}$$

Thus, it is virtually the same as the resistivity due to the e-e mode, implying negligible additional heating.

The final case to be discussed here is the one with an initial density of $8 \times 10^{13}/\text{cm}^3$ and temperature 2 eV. The beam was 1 MeV and 50 kA. At this low plasma density, the growth rate δ exceeds the collision frequency very early in the rise time of the current pulse. Therefore, we take half the beam maximum density $(6 \times 10^{11}/\text{cm}^3)$ and $\gamma = 2$ in order to obtain the δ to use in calculating $\Delta\epsilon_0$. We obtain $\delta/\omega_p \approx 2 \times 10^{-2}$ and $\Delta\epsilon_0 \approx 1.0 \times 10^{16}$ eV/cm^3. During the next stage of the heating $\delta/\omega_p \approx 3 \times 10^{-3}$. However, we now have the additional complication of a significant change in the plasma density and temperature during the course of the interaction. The wave and resistive energy deposition between 20 and 70 nsec can be written

$$\Delta\epsilon_1 \approx 2 \times 10^{24} \int_{20}^{70} \frac{T_e(t)\, dt \times 10^{-9}}{(n_p(t)/8 \times 10^{13}\ \text{cm}^{-3})^{3/2}} \frac{\text{eV}}{\text{cm}^3} \ , \tag{16a}$$

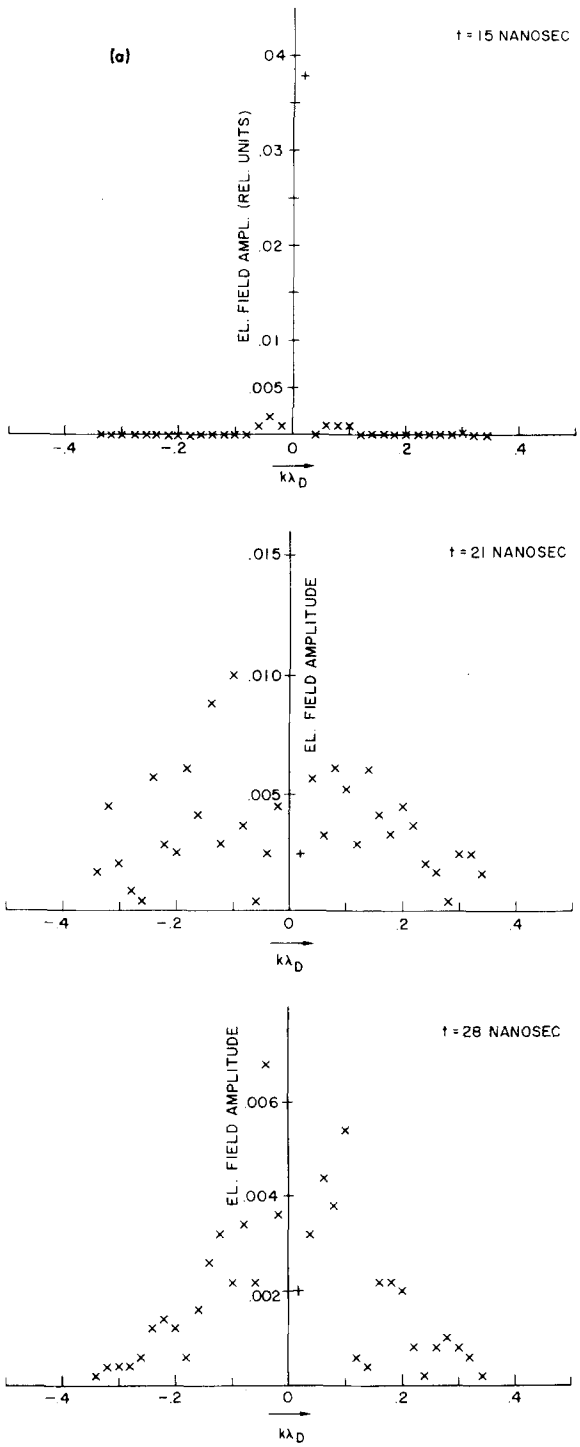

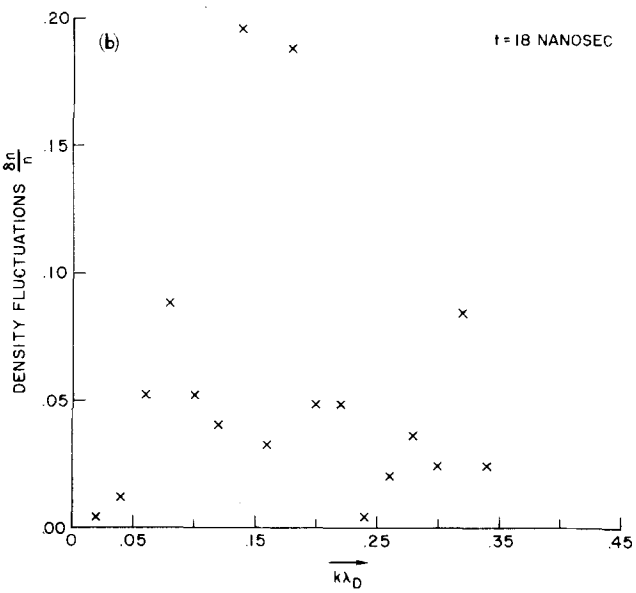

FIG. 19 (a) High frequency (ω_p) and (b) low frequency ($< \omega_{pi}$) spectra from the numerical simulation for the highly ionized case. The waves in resonance with the beam are indicated by +.

$$\Delta\epsilon_2 \approx 2\times 10^{18} \int_{20}^{70} \frac{j^2\, dt \times 10^{-9}}{(n_p(t)/8\times 10^{13}\ \mathrm{cm}^{-3})^{3/2}} \frac{\mathrm{eV}}{\mathrm{cm}^3}\ , \qquad (16b)$$

From Fig. 11 we take $T_e \approx 30$ eV as an average over that time interval, and approximate the density by $n_p(t) \approx 8 \times 10^{13}(1+0.12\,t)$, where t is in nsec. This gives

$$\Delta\epsilon_1 \approx 3\times 10^{17}\ \mathrm{eV/cm^3}\ ;\ \ \Delta\epsilon_2 \approx 4\times 10^{16}\ \mathrm{eV/cm^3}\ ,$$

for a total predicted energy deposition of 3.5×10^{17} eV/cm^3. Assuming uniform energy deposition over the 20 cm^2 beam area, this is a factor of three greater than the value we would estimate from the results shown in Fig. 11 (including the 40 eV ionization energy and the 2.5 area factor).

Again checking the possibility of ion acoustic resistive heating, the coefficient of j^2 in Eq. (16b) in a factor of 5 greater than the value of η_{ia} at $n_p = 8\times 10^{13}$/cm^3, obtained from Eq. (15). However, $\eta_{ia} \propto 1/n_p^{1/2}$ whereas e-e mode resistivity is evidently proportional to $n_p^{-3/2}$. Thus, these resistivities are about equal at 4×10^{14}/cm^3, which is reached at about 50 nsec. Since most of the contribution to $\Delta\epsilon_2$ is made by this time (because of the inverse dependence on density for both resistivities),

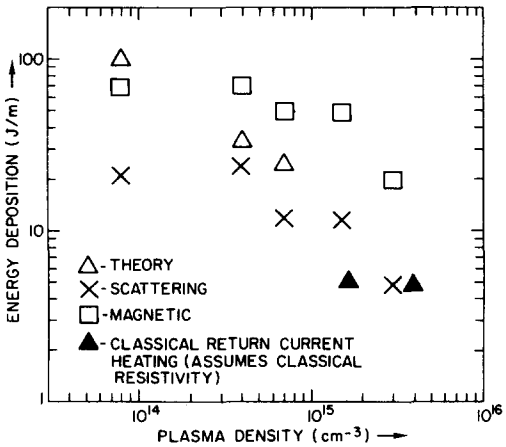

FIG. 20. Energy deposition as a function of plasma density: a comparison of experimental observations and theoretical predictions. Note that the two lower density cases are partially ionized helium and the other three are highly ionized hydrogen. The two higher density theory points are classical return current heating predictions since the two stream instability is predicted to be stable at these densities.

and since $\Delta\epsilon_2 \ll \Delta\epsilon_1$, ion acoustic turbulence will again contribute only a small amount to the total deposited energy.

In Fig. 20, we plot the theoretically predicted energy deposition as a function of plasma density for the three cases considered. Also shown on the graph are the experimental results from scattering and from magnetic diagnostics. The quantitative agreement is quite reasonable considering the difficulties in making the theoretical estimates. We emphasize that this comparison is a result of including the early and late stages of the interaction, and is not scaled. By contrast, the quasi-hydrodynamic formulation of Thode[34] gives good agreement with the scaling of plasma heating by an intense beam as a function of beam and plasma parameters. Quantitatively, Thode predicts much greater energy deposition than most experiments observe (including the present one), presumably because he considers only the early stages of the interaction, when it is strongest.

VI. CONCLUSIONS

In this paper, we have presented experimental results for plasma heating by an intense relativistic electron beam. The initial plasma density range from 5×10^{13}/cm^3 to 4×10^{15}/cm^3, the lower density cases being partially ionized and the higher density cases highly ionized. In all cases, the energy coupled from the beam to the plasma is greater than can be explained by binary collisions between beam electrons and plasma particles. At the highest plasma densities, classical damping of the beam induced return current is adequate to explain the observed heating. However, over most of the plasma density range tested, i.e., less than 1.5×10^{15}/cm^3, using a 2 kA/cm^2 beam, the plasma heating by the beam cannot be explained by classical processes. These results are found to be explained qualitatively and quantitatively by the use of a full nonlinear treatment of the electron-electron two-stream instability in the kinetic regime.

The results of this experiment, namely, 2–7%/m energy coupling efficiency, at beam to plasma density ratios n_b/n_p in the range 10^{-4}–10^{-2} are consistent with results of previous experiments with comparable beam and plasma parameters.[12–20,26,59] Similar conclusions as to the energy coupling mechanism, namely, the electron-electron instability, have been reached in most of these experiments. However, the use of more detailed diagnostics, and a more uniform interaction geometry in the present experiment, and a complete nonlinear treatment of the e-e mode instability for comparison with theory, have provided strong confirmation for the presence of this instability.

We should also note that the theory we have used predicts that return current heating due to the parametrically generated ion waves W_a will be dominant for higher beam current densities.[33] This has been tentatively confirmed in recently presented preliminary results.[60,80]

Presuming that the agreement between theory and experiment is not fortuitous, it is interesting to note a particular implication of our theoretical discussion. Equation (10) for the wave energy transfer rate during the later stages of the interaction, when combined with Eq. (12), implies a rate which increases linearly with plasma temperature (at constant densities)

$$d\epsilon_1/dt = 32(\delta^2/\omega_p) n_p T_e \ .$$

Thus, as the plasma heats, the coupling efficiency via this mechanism increases. This implies that the use of 1 μsec pulse beams should be advantageous for heating plasma in a long solenoidal system of the type suggested by Benford *et al.*[9] This equation also implies that the coupling efficiency of the entire beam will be increased if the plasma can be preheated to a higher temperature.

ACKNOWLEDGMENTS

During the course of this work, a large number of people have provided us with many helpful discussions and assistance. For example, I. Haber provided important assistance in the construction of the atomic physics computational model for the explanation of the partially ionized experiments, as well as in preparation of the results presented in Figs. 18 and 19. R. E. Kribel, C. Ekdahl, K. R. Chu, A. E. Robson, R. N. Sudan, and many others have participated in fruitful discussions of this work with us. The engineering support required by this experiment was provided by J. K. Burton, D. Conte, W. H. Lupton, and M. P. Young. Technical assistance was provided by R. M. Jones, J. R. Singer, and J. M. Vary. Initial work on the Thomson scattering system was done by R. H. Dixon and J. L. Ford.

Finally, we would like to acknowledge the support, encouragement and interest of R. Shanny during the entire course of this work.

APPENDIX

In order to understand the observed time dependence of the plasma density and temperature in the partially

ionized helium experiments described in Sec. IV B, we have solved the following set of coupled differential equation:

$$dn_0/dt = -n_p n_0 S_1 + n_p n_+(\alpha_r^+ + \alpha_3^+ n_e) \ , \tag{A1}$$

$$dn_+/dt = -dn_0/dt - n_p n_+ S_2 + n_p n_{++}(\alpha_r^{++} + \alpha_3^{++} n_p) \ , \tag{A2}$$

$$n_{++} = N - n_0 - n_+ \ , \tag{A3}$$

$$n_p = n_+ + 2n_{++} \ , \tag{A4}$$

$$\frac{d}{dt}(\tfrac{3}{2} n_p T_e) = Q - n_p n_0 S_1 E_1 - n_p n_+ S_2 E_2 - n_p n_0 \sum_{\text{He-I}} X_i E_i - n_p n_+ \sum_{\text{He-II}} X_j E_j - P_B - Q_+ - Q_{++} - \tfrac{3}{2} n_p T_e \times (n_+ \alpha_r^+ + n_{++}\alpha_r^{++}) + n_p^2(\tfrac{3}{2} T_e + \bar{E})(n_+ \alpha_3^+ + n_{++}\alpha_3^{++}) \ , \tag{A5}$$

$$(d/dt)(\tfrac{3}{2} n_+ T_+) = Q_+ \ , \tag{A6}$$

$$(d/dt)(\tfrac{3}{2} n_{++} T_{++}) = Q_{++} \ . \tag{A7}$$

In these equations we are considering atomic processes only, neglecting all plasma dynamical, kinetic, and transport processes (such as expansion, end loss, etc.). This is equivalent to considering the plasma to be spatially uniform on the timescale and spatial scale of interest. These ideas are consistent with the low temperature observed and classical transport and thermal expansion. In solving these equations we assume a Maxwellian velocity distribution for the free electrons and ions.

The first three equations describe the time development of the neutral, singly and doubly ionized helium densities, n_0, n_+, and n_{++}, respectively, in terms of the electron density n_p and the various rate coefficients. S_1 and S_2 are the ionization rate coefficients for neutral and singly ionized helium, respectively, α_r^+ and α_r^{++} are the radiative recombination coefficients for singly and twice ionized helium, and α_3^+ and α_3^{++} are the three-body recombination coefficients. Expressions for S_1 and S_2 are from Drawin,[71] which agree well with the calculations of Lotz.[72] Adjustments are made to these coefficients to account for ionization from the upper levels of the resonance lines. The radiative recombination coefficients used are those given by Seaton[81] (α_r^+) and Burgess and Seaton[82] (α_r^{++}), and a hydrogenic expression[83] has been utilized for the three body recombination coefficient. Equations (A3) and (A4) indicate the conservation of heavy particles (100 mTorr He implies $N \approx 3.5 \times 10^{15}/\text{cm}^3$) and charge neutrality, respectively.

Equations (A5)–(A7), when combined with Eqs. (A1)–(A4), give the time dependence of the electron temperature T_e, and the singly and doubly ionized helium temperatures, T_+ and T_{++}, respectively. The terms on the right-hand side of Eq. (A5) are, in order: (1) the heat source term for the electrons, usually taken to be a single resistive term, ηj^2, where η is the resistivity and j is the plasma current density; power loss due to ionization of (2) helium atoms and (3) singly ionized helium, where the ionization energies are $E_1 = 24.6$ eV and $E_2 = 54.4$ eV; power loss due to inelastic electron impact excitation of (4) helium atoms (He-I), including radiative and metastable states, and (5) singly ionized helium (He-II), where E_i is the threshold energy for excitation of the ith state with an excitation rate coefficient X_i; (6) power loss due to bremsstrahlung; energy transfer rate between the electrons and (7) singly charged ions and (8) doubly charged ions (loss rates so long as $T_e > T_+, T_{++}$); (9) power loss due to radiative recombination of singly and doubly ionized helium; and (10) power gain due to three body recombination of singly and doubly ionized helium where $\bar{E}$ is an average energy per recombination (taken to be 0.25 E_1 and 0.25 E_2 for the two species). The excitation rate coefficient X_i are from Drawin[71] for energy loss to allowed transitions. The coefficients for the metastable states of helium are obtained[84] from measured cross sections.[85,86] The bremsstrahlung power coefficient used is the value given by Spitzer[87] and the electron ion energy transfer rates are obtained from the classical formula given by Braginskii.[88]

The resistivity used in the energy source term $Q = \eta j^2$ in Eq. (A5) consisted of the sum of three terms: (1) classical resistivity η_{cl}, (2) resistivity due to ion acoustic turbulence, η_{ia}, as determined from the experimental results of Zavoiskiy *et al.*,[79] and (3) resistivity due to electron-electron two-stream instability turbulence, η_{ee}, as discussed in Sec. V. Specific values used, in units such that when multiplied by j^2, with j in kA/cm^2, the product is in eV/cm^3 – sec, were

$$\eta_{cl} = 6 \times 10^{22}\left(\frac{\ln \Lambda}{T_e^{3/2}} + \frac{0.005\, n_0}{n_p}\right) \ , \tag{A8}$$

$$\eta_{ia} = 3 \times 10^{30}/\sqrt{n_p} \ , \tag{A9}$$

$$\eta_{ee} = 5 \times 10^{32}(n_b/n_p^{3/2}) \ . \tag{A10}$$

In these equations, temperatures are in eV and densities in cm^{-3}. The first term in η_{cl} is from Spitzer,[87] $\ln \Lambda$ being the usual Coulomb logarithm, and the second term is the resistivity due to electron-neutral collisions, and it is approximated using the elastic collision cross section given by Brown.[89] The effective collision frequency due to ion acoustic turbulence implied by Eq. (A9) is about $\omega_p/80$, where ω_p is the plasma frequency. Since $T_e \gg T_+, T_{++}$ whenever plasma current is flowing in the partially ionized He calculations described here, η_{ia} is cut off when the plasma electron drift speed drops below the sound speed $c_s = (T_e/M)^{1/2}$, where M is the mass of the helium ion, as per the discussions in the main text.

By far the most important ionization and energy loss terms in Eqs. (A1), (A2), and (A5) for the partially ionized helium calculations for which results were given in Sec. IV B were those involving ionization of, and line radiation from, neutral helium. Therefore, we also give the specific coefficients used for these terms, in units of eV-cm^3/sec:

$$S_1 = 2.35 \times 10^{-7}\, \Psi(24.6)\, \exp(-24.6/T_e)/\sqrt{T_e} \ , \tag{A11}$$

$$\sum_{\text{He-I}} X_i E_i = 4.3 \times 10^{-6}[0.276\, \Psi(21.1)\, \exp(-21.1/T_e) + 0.2\, \Psi(22.9) \exp(-22.0/T_e)/\sqrt{T_e}] + 2.33 \exp(-20/T_e)(4.7 \times 10^{-9} + 4.6 \times 10^{-10} T_e - 1.2 \times 10^{-11} T_e^2) \ , \tag{A12}$$

where T_e is in eV and

$$\Psi(X) = \frac{1}{1+X/T_e}\left\{\frac{1}{20+X/T_e} + \ln[1.2(1+T_e/X)]\right\} .$$

The first set of terms in Eq. (A12) represents the most important optical transitions, and the second set of terms represents metastable transitions.

Equations (A1)–(A7) were solved using a computational scheme developed by Boris and Winsor.[90]

Calculated electron density and temperature even at early time (~10 nsec) were found to be independent of initial electron temperature over the range 1–5 eV and ion temperatures from 0.1–1 eV. Changes of the order of 25% in initial density did affect early time temperature (lower initial density giving higher peak temperatures, see Figs. 11 and 12, and conversely), but only small changes in electron density and temperature for $t \gtrsim 100$ nsec were obtained.

[1]J. C. Martin, T. H. Storr, M. J. Goodman, and D. W. Forster (private communication).

[2]T. H. Martin, J. P. VanDevender, D. L. Johnson, D. H. McDaniel, and M. Aker, in *Proceedings of the International Topical Conference on Electron Beam Research and Technology*, edited by G. Yonas (Sandia Laboratories, Albuquerque, N. M., 1976), Vol. 1, p. 450, and references therein.

[3]J. J. Clark, M. Ury, M. L. Andrews, D. A. Hammer, and S. Linke, in *Record of the Tenth Symposium on Electron, Ion and Laser Beam Technology*, edited by L. Marton (San Francisco Press, San Francisco, 1969), p. 117.

[4]B. Bernstein and I. Smith, IEEE Trans. Nucl. Sci. NS-18, 294 (1971).

[5]For a general discussion with many references, see L. S. Levine and M. Ury, IEEE Trans. Nucl. Sci. NS-20, 456 (1973).

[6]J. Chang, L. P. Mix, F. C. Perry, M. M. Widner, and J. W. Poukey, in *Proceedings of the International Topical Conference on Electron Beam Research and Technology*, edited by G. Yonas (Sandia Laboratories, Albuquerque, N. M., 1976), Vol. 1, p. 82, and references therein.

[7]G. Yonas, J. W. Poukey, K. R. Prestwich, J. R. Freeman, A. J. Toepfer, and M. J. Clauser, Nucl. Fusion **14**, 731 (1974).

[8]C. Stallings, R. Schneider, and D. Cummings, in *Proceedings of the International Topical Conference on Electron Beam Research and Technology*, edited by G. Yonas (Sandia Laboratories, Albuquerque, N. M., 1976), Vol. 1, p. 364.

[9]J. Benford, T. S. T. Young, B. Ecker, D. Dakin, I. Smith, S. Putnam, and V. Bailey, in *Proceedings of the International Topical Conference on Electron Beam Research and Technology*, edited by G. Yonas (Sandia Laboratories, Albuquerque, N. M., 1976), Vol. 2, p. 476.

[10]Beam injection into toroidal geometry has been investigated by J. Benford, B. Ecker, and V. Bailey, Phys. Rev. Lett. **33**, 574 (1974); P. Gilad, B. R. Kusse, and T. R. Lockner, Phys. Rev. Lett. **33**, 1275 (1974); and Phys. Fluids **18**, 607 (1975); and M. Masuzaki, A. Mohri, T. Tsuzuki, and K. Ikuta, in *Proceedings of the International Topical Conference on Electron Beam Research and Technology*, edited by G. Yonas (Sandia Laboratories, Albuquerque, N. M. 1976), Vol. 2, p. 435.

[11]D. A. Hammer and K. Papadopoulos, Nucl. Fusion **15**, 977 (1975).

[12]A. T. Altyntsev, A. G. Eskov, O. A. Zolotovskii, V. I. Koroteev, R. Kh. Kurtmullaev, V. D. Masalov, and V. N. Semenov, Zh. Eksp. Teor. Fiz., Pisma Red. **13**, 197 (1971)[JETP Lett. **13**, 139 (1971)]; A. T. Altyntsev, B. N. Breizman, A. G. Eskov, O. A. Zolotovskii, V. I. Koroteev, R. Kh. Kurtmulaev, V. D. Masalov, D. D. Ryutov, and V. N. Semenov, in *Plama Physics and Controlled Nuclear Fusion Research* (International Atomic Energy Agency, Vienna, 1971), Vol. II, p. 309.

[13]D. R. Smith, Phys. Lett. A **42**, 211 (1972).

[14]C. A. Kapetanakos and D. A. Hammer, Appl. Phys. Lett. **23**, 17 (1973).

[15]P. A. Miller and G. W. Kuswa, Phys. Rev. Lett. **30**, 958 (1973).

[16]Yu. I. Abrashitov, V. S. Koydan, V. V. Konyukhov, V. M. Lagunov, V. N. Luk'yanov, and K. I. Mekler, Zh. Eksp. Teor. Fiz., Pis'ma Red. **18**, 675 (1973) [JETP Lett. **18**, 395 (1973)]; Yu. I. Abrashitov, V. S. Koydan, V. V. Konyukhov, V. M. Lagunov, V. N. Luk'yanov, and K. I. Mekler, and D. D. Ryutov, Zh. Eksp. Teor. Fiz. **66**, 1324 (1974) [Sov. Phys.-JETP **39**, 647 (1975)].

[17]A. V. Arzhannikov, B. N. Breizman, L. N. Vyacheslavov, V. S. Koydan, V. V. Konyukhov, and D. D. Ryutov, in *Plasma Physics and Controlled Nuclear Fusion Research* (International Atomic Energy Agency, Vienna, 1975), Vol. III, p. 257.

[18]P. Korn, F. Sandel, and C. B. Wharton, Phys. Rev. Lett. **31**, 579 (1973); J. Appl. Phys. **44**, 4946 (1973).

[19]C. Ekdahl, M. Greenspan, R. E. Kribel, J. Sethian, and C. B. Wharton, Phys. Rev. Lett. **33**, 346 (1974).

[20]P. A. Miller, Appl. Phys. Lett. **27**, 107 (1975).

[21]J. P. VanDevender, J. D. Kilkenny, and A. E. Dangor, Phys. Rev. Lett. **33**, 689 (1974); J. Appl. Phys. **47**, 1955 (1976).

[22]D. Prono, B. Ecker, N. Bergstrom, and J. Benford, Phys. Rev. Lett. **35**, 438 (1975).

[23]C. A. Kapetanakos, W. M. Black, and K. R. Chu, Phys. Rev. Lett. **34**, 1156 (1975).

[24]G. C. Goldenbaum, W. F. Dove, K. A. Gerber, and B. G. Logan, Phys. Rev. Lett. **32**, 830 (1974): B. G. Logan, W. F. Dove, K. A. Gerber, and G. C. Goldenbaum, IEEE Trans. Plasma Sci. **2**, 182 (1974).

[25]W. F. Dove, K. A. Gerber, and D. A. Hammer, Appl. Phys. Lett. **28**, 173 (1976).

[26]R. Okamura, Y. Nakamura, and N. Kawashima, Appl. Phys. Lett. **28**, 701 (1976).

[27]R. E. Lee and R. N. Sudan, Phys. Fluids **14**, 1213 (1971).

[28]B. N. Breizman and D. D. Ryutov, Nucl. Fusion **14**, 873 (1974).

[29]Ya. B. Fainberg, V. D. Shapiro, and V. I. Shevchenko, Zh. Eksp. Teor. Fiz. **57**, 966 (1969) [Sov. Phys.-JETP **30**, 528 (1970)].

[30]L. E. Thode and R. N. Sudan, Phys. Rev. Lett. **30**, 732 (1973); Phys. Fluids **18**, 1552 (1975).

[31]L. I. Rudakov, Zh. Eksp. Teor. Fiz. **59**, 2091 (1970) [Sov. Phys.-JETP **32**, 1134 (1971)].

[32]R. L. Ferch and R. N. Sudan, Plasma Phys. **17**, 905 (1975).

[33]K. Papadopoulos, Phys. Fluids **18**, 1769 (1975).

[34]L. E. Thode, Phys. Fluids **19**, 305 (1976); **19**, 831 (1976).

[35]A. J. Toepfer and J. W. Poukey, Phys. Lett. A **42**, 383 (1973); Phys. Fluids **16**, 1546 (1973).

[36]L. E. Thode and B. B. Godfrey, Phys. Fluids **19**, 316 (1976); B. B. Godfrey, W. R. Shanahan, and L. E. Thode, *ibid.* **18**, 346 (1975).

[37]D. A. Hammer and N. Rostoker, Phys. Fluids **13**, 1831 (1970).

[38]J. L. Cox and W. H. Bennett, Phys. Fluids **13**, 182 (1970).

[39]K. R. Chu and N. Rostoker, Phys. Fluids **16**, 1472 (1973).

[40]G. Kuppers, A. Slat, and H. K. Wimmel, Plasma Phys. **15**, 429 (1973).

[41]J. D. Lawson, J. Electron. Control **3**, 587 (1957); **5**, 146 (1958); J. Nucl. Energy, Pt. C. **1**, 31 (1959).

[42]Yonas and P. Spence, in *Record of the Tenth Symposium on Electron, Ion and Laser Beam Technology*, edited by L. Marton (San Francisco Press, San Francisco, 1969), p. 143.

[43]K. R. Chu, C. A. Kapetanakos, and R. W. Clark, Appl. Phys. Lett. **27**, 185 (1975).
[44]K. R. Chu, R. W. Clark, M. Lampe, P. C. Liewer, and W. M. Manheimer, Phys. Rev. Lett. **35**, 94 (1975).
[45]R. V. Lovelace and R. N. Sudan, Phys. Rev. Lett. **27**, 1256 (1971).
[46]L. E. Thode and R. N. Sudan, Phys. Fluids **18**, 1564 (1975).
[47]H. Alfvén, Phys. Rev. **55**, 425 (1939).
[48]C. A. Kapetanakos, W. M. Black, and C. D. Striffler, Appl. Phys. Lett. **26**, 368 (1975).
[49]W. H. Bennett, Phys. Rev. **45**, 890 (1934); **98**, 1584 (1955).
[50]K. R. Chu and N. Rostoker, Phys. Fluids **17**, 813 (1974); K. Molvig and N. Rostoker, *ibid.* **20**, 494 (1977); **20**, 510 (1977).
[51]K. R. Chu and R. W. Clark (to be published).
[52]T. G. Roberts and W. H. Bennett, Plasma Phys. **10**, 381 (1968).
[53]J. Benford and B. Ecker, Phys. Fluids **15**, 366 (1972).
[54]L. S. Levine, I. M. Vitkovitsky, D. A. Hammer, and M. L. Andrews, J. Appl. Phys. **42**, 1863 (1971).
[55]M. L. Andrews, H. E. Davitian, D. A. Hammer, H. H. Fleischmann, J. A. Nation, and N. Rostoker, Appl. Phys. Lett. **16**, 98 (1970).
[56]S. E. Graybill, IEEE Trans. Nucl. Sci. **NS-18**, 438 (1971).
[57]C. A. Kapetanakos and C. D. Striffler, J. Appl. Phys. **46**, 2509 (1975).
[58]M. Friedman and M. Ury, Rev. Sci. Instrum. **41**, 1334 (1970).
[59]C. Ekdahl, M. Greenspan, J. Sethian, and C. B. Wharton, Bull. Am. Phys. Soc. **20**, 1270 (1975); J. D. Sethian, C. Ekdahl, and C. B. Wharton, Bull. Am. Phys. Soc. **21**, 674 (1976); J. D. Sethian and C. Ekdahl (to be published).
[60]M. Greenspan, C. Ekdahl, J. Sethian, and C. B. Wharton, Bull. Am. Phys. Soc. **20**, 1271 (1976); M. Greenspan, PhD. thesis, Cornell University (1976).
[61]J. K. Burton, J. J. Condon, M. D. Jevnager, W. H. Lupton, and T. J. O'Connell, in *Proceedings of the Fifth Symposium on Engineering Problems of Fusion Research* (IEEE, New York, 1974), p. 613.
[62]R. K. Parker, R. E. Anderson, and C. V. Duncan, J. Appl. Phys. **45**, 2463 (1974).
[63]D. Pellinen, Rev. Sci. Instrum. **41**, 1347 (1970).
[64]R. Lee and M. Lampe, Phys. Rev. Lett. **31**, 1390 (1973); K. Molvig, *ibid.* **35**, 1504 (1975).
[65]H. R. Griem, *Plasma Spectroscopy* (McGraw-Hill, New York, 1964), p. 309.
[66]J. Sheffield, *Plasma Scattering of Electromagnetic Radiation* (Academic, New York, 1975).
[67]K. A. Gerber, Naval Research Laboratory Memorandum Report 2818 (1974).
[68]D. A. Hammer, K. A. Gerber, W. F. Dove, G. C. Goldenbaum, B. G. Logan, K. Papadopoulos, and A. W. Ali, Naval Research Laboratory Memorandum Report 3439 (1977).
[69]L. E. Aranchuk, E. K. Zavoiskii, D. N. Lin, and L. I. Rudakov, Zh. Eksp. Teor. Fiz. Pis'ma Red. **15**, 33 (1972) [JETP Lett. **15**, 22 (1972)].
[70]M. N. Rosenbluth and C. S. Liu, Phys. Fluids **19**, 815 (1976).
[71]H. W. Drawin, Euratron Special Report EUR-CEA-FC-383 (1966), revised (1967).
[72]W. Lotz, Astrophys. J. Suppl. **14**, 207 (1967).
[73]K. Papadopoulos, M. L. Goldstein, and R. A. Smith, Astrophys. J. **190**, 175 (1974).
[74]V. N. Tsytovich, Physics C **82**, 141 (1976).
[75]W. Manheimer and K. Papadopoulos, Phys. Fluids **18**, 1397 (1975).
[76]J. Dawson and C. Oberman, Phys. Fluids **5**, 517 (1962); **6**, 394 (1963).
[77]K. Papadopoulos and T. P. Coffey, J. Geophys. Res. **79**, 1558 (1974).
[78]P. J. Palmadesso, T. P. Coffey, I. Haber, and K. Papadopoulos, Bull. Am. Phys. Soc. **20**, 1277 (1975); H. Rowland and K. Papadopoulos, *ibid.* **21**, 1170 (1976).
[79]E. K. Zavoisky, B. A. Demidov, Yu. G. Kalinin, A. G. Plakhov, L. I. Rudakov, V. E. Rusanov, V. A. Skoryupin, G. Ye. Smoklin, A. V. Titov, S. D. Franchenko, V. V. Shapkin, and G. V. Sholin, in *Plasma Physics and Controlled Nuclear Fusion Research* (International Atomic Energy Agency, Vienna, 1971), Vol. II, p. 3.
[80]A. K. L. Dymore-Bradshaw, A. E. Dangor, and J. D. Kilkenny, in *Plasma Physics and Controlled Nuclear Fusion Research* (International Atomic Energy Agency, Vienna, 1977), Vol. II, p. 555.
[81]M. J. Seaton, Mon. Not. Astron. Soc. **119**, 81 (1959).
[82]A. Burgess and M. J. Seaton, Mon. Not. Astron. Soc. **121**, 76 (1960).
[83]Y. B. Zeldovitch and Y. P. Raizer, *Physics of Shock Waves and High Temperature Hydrodynamic Phenomena* (Academic, New York, 1966), Vol. 1, p. 407.
[84]A. W. Ali and A. D. Anderson (private communication).
[85]C. R. Lloyd, E. Weigold, P. J. O. Teubner, and S. T. Hood, J. Phys. B **5**, 1712 (1972).
[86]W. L. Borst, Phys. Rev. A **9**, 1195 (1974).
[87]L. Spitzer, Jr., *Physics of Fully Ionized Gases* (Interscience, New York, 1967).
[88]S. I. Braginskii, in *Reviews of Plasmas Physics*, edited by M. A. Leontovich (Consultants Bureau, New York, 1965), Vol. 1, p. 217.
[89]S. C. Brown, *Basic Data of Plasma Physics* (MIT Press, Cambridge, 1967), p. 17.
[90]J. P. Boris and N. Winsor, Princeton Plasma Physics Laboratory Report MATT-652 (1970).